alcoholic liver diseases (3, 8). On the other hand, several recent large-scale studies have indicated that coffee drinking suppressed the progression of liver fibrosis and inhibited the development of hepatocellular carcinoma (18, 19).

The fact that liver cirrhosis is not a necessary condition for hepatocellular carcinoma occurrence was already known, not only from clinical findings but also from genetic findings. Among hepatocellular carcinoma cases with HBV, a part of the HBV genome has been shown to be integrated into the host's intracellular DNA, thereby causing hepatocellular carcinoma (20). Among hepatocellular carcinoma cases with HCV, the HCV core protein seems to directly contribute to the mechanism of carcinogenesis by elevating oxidative stress (21). In light of the aforementioned findings, for the purpose of determining independent risk factors for hepatocellular carcinoma, careful analyses are needed controlling for severity of liver fibrosis, as well as for viral etiologic factors.

With the aim of determining whether HBV or HCV infections, alcohol consumption, smoking, coffee drinking, BMI, and diabetes mellitus are independent risk factors for hepatocellular carcinoma, and how the effects of these factors might change after adjusting for severity of liver fibrosis, we conducted a nested case-control study among the Adult Health Study longitudinal cohort using stored sera. We also evaluated whether viral etiology and increase of BMI exert synergistic effects on the risk for hepatocellular carcinoma.

Materials and Methods

Cohorts. The Atomic Bomb Casualty Commission and its successor, the Radiation Effects Research Foundation, established the Adult Health Study longitudinal cohort in 1958, in which 20,000 age-, gender-, and city-matched proximal and distal atomic bomb survivors and persons not present in the cities at the time of bombings have been examined biennially in outpatient clinics in Hiroshima and Nagasaki.

Study Population. Serum samples obtained from the study participants on each occasion of visiting outpatient clinics have been collected and stored systematically since 1969 (22). Incident cancer cases were identified through the Hiroshima Tumor and Tissue Registry and Nagasaki Cancer Registry, supplemented by additional cases detected via pathologic review of related diseases (23). There were 359 primary hepatocellular carcinoma cases among Adult Health Study participants diagnosed between 1970 and 2002, who visited our outpatient clinics before their diagnosis. Of these, 130 cases were excluded because of nonavailability of stored serum or having only one stored sample. The other 229 cases had serum samples obtained within 6 years before hepatocellular carcinoma diagnosis. After excluding five cases with inadequate stored serum, 224 cases remained for our study. For each case, three controls were selected from the cohort in nested case-control fashion. Nested control selection was random among those who matched the case on gender, age (±2 years), city, time of serum storage (±2 years), and method of serum storage, and countermatched on radiation exposure (24). Although the total number of potential matched control serum samples is 672, because of occasional lack of subjects with stored sera who met the matching and countermatching criteria, the total number of control serum samples actually used was 644.

Laboratory Tests. HBV surface antigen and antibody to hepatitis B core antigen were measured by enzyme immunoassay, and anti-HCV antibody was measured by second-generation enzyme immunoassay as previously described (22, 25). Qualitative detection of HCV RNA among anti-HCV–positive samples was done using a thermocycler (Whatman Biometra) with two sets of PCR primers corresponding to the 5′-untranslated region, as previously described (25). Qualitative detection of HCV RNA was conducted at least twice. HBV infection (HBV+) status was defined as positive for HBV surface antigen or having a high titer of the antibody to hepatitis B core antigen. HCV infection (HCV+) status was defined as positive for HCV RNA (25). Hyaluronic acid and type IV collagen as liver fibrosis markers were measured using an autoanalyzer (Hitachi 7180, Hitachi, Ltd.) and latex agglutination–turbidimetric immunoassay (Fujirebio, Inc., Daiichi Pure Chemicals Co. Ltd.). Ferritin was measured using an autoanalyzer (Hitachi 7180, Hitachi) and colloidal gold immunoassay (Alfresa Pharma Corporation). Platelet count was measured using an automatic blood cell counter at the time of serum storage.

Information on Covariates. Self-administered questionnaires on various lifestyle factors were given to participants in 1965 during attendance at the Adult Health Study examination and in 1978 by mail survey. Information from the 1978 survey was obtained before hepatocellular carcinoma diagnosis for all but 19 (15%) of the cases. Information on alcohol consumption was obtained from the 1965 questionnaire when available, with missing data complemented using the 1978 survey. Alcohol consumption per volume of each type of alcoholic beverage was quantified as previously described (26), and mean ethanol amounts were calculated as grams per day. Information on smoking habits was obtained from the 1965 questionnaire; subjects were divided into the following categories: never, prior, and current smoker. Information on coffee drinking was obtained from the 1978 survey; subjects were divided into the following categories of frequency of coffee consumption: never, 1 day per week, 2 to 4 days per week, and almost daily. Disease diagnoses were based on the International Classification of Diseases (ICD) codes: diabetes mellitus was defined by ICD-7 code 260, ICD-8 code 250, ICD-9 code 250, and ICD-10 codes E10 through E14. BMI (kg/m^2) was calculated from height and weight measured at the Adult Health Study examination.

Subjects were classified based on BMI quintiles with cut points of 19.5, 21.2, 22.9, and 25.0. The number of hepatocellular carcinoma cases with BMI of >30.0 kg/m^2 was too small to be analyzed in detail. Following the recommendations for Asian people by the WHO, the International Association for the Study of Obesity, and the International Obesity Task Force (27), 21.3 to 22.9 kg/m^2 was considered as normal, 23 to 25 kg/m^2 as overweight, and >25.0 kg/m^2 as obese in the present study. We used information on diabetes mellitus and BMI obtained 10 years before the time of hepatocellular

Table 1. Characteristics of hepatocellular carcinoma cases and controls

Study variables	Hepatocellular carcinoma cases (n = 224)			Controls (n = 644)		
	Complete data (%)	n (%)	Mean (SD)	Complete data (%)	n (%)	Mean (SD)
Matched variables						
Gender	100			100		
Male		136 (60.7)			387 (60.1)	
Female		88 (39.3)			257 (39.9)	
Age at hepatocellular carcinoma diagnosis (y)	100		67.6 (10.1)	—		—
City	100			100		
Hiroshima		155 (69.2)			444 (68.9)	
Nagasaki		69 (30.8)			200 (31.1)	
Age at serum storage (y)	100		66.4 (10.2)	100		63.7 (9.8)
Unmatched variables						
Etiology (HBV/HCV status)	94.2			99.4		
HBV−/HCV−		45 (21.3)			579 (90.5)	
HBV+/HCV−		29 (13.7)			18 (2.8)	
HBV−/HCV+		132 (62.6)			41 (6.4)	
HBV+/HCV+		5 (2.4)			2 (0.3)	
Fibrosis markers	94.2			99.4		
Hyaluronic acid (ng/mL)			288.6 (284.6)			69.1 (108.3)
Type IV collagen (ng/mL)			245.2 (136.9)			148.8 (122.1)
Platelet count ($\times 10^4/\mu L$)	67.4		13.0 (6.0)	70.0		22.4 (6.2)
Ferritin (ng/mL)	92.0		250.5 (278.6)	98.6		136.7 (151.0)
Alcohol consumption (g of ethanol per day)	88.8			89.6		
>0 and <20		37 (18.6)			130 (22.5)	
≥20 and <40		20 (10.1)			64 (11.1)	
≥40		45 (22.6)			68 (11.8)	
Current smoking		107 (53.8)			262 (45.3)	
Prior smoking	88.8	12 (6.0)		89.8	33 (5.7)	
Daily coffee drinking	62.1	38 (27.3)		73.3	175 (37.1)	
BMI (kg/m^2) 10 y before diagnosis	93.8			98.3		
≤19.5		38 (18.1)			122 (19.3)	
19.6-21.2		33 (15.7)			136 (21.5)	
21.3-22.9		36 (17.2)			142 (22.4)	
23-25		49 (23.3)			124 (19.6)	
>25		54 (25.7)			109 (17.2)	
Diabetes 10 y before diagnosis	100	18 (8.0)		100	33 (5.1)	
Radiation dose to the liver (Gy)	91.1		0.46 (0.69)	94.1		0.34 (0.56)

carcinoma diagnosis or control matching because these conditions are subject to change because of disease progression in the later stages before diagnosis of hepatocellular carcinoma. Atomic bomb radiation dose was estimated for each subject according to the Dosimetry System DS02 (28).

Ethical Consideration. This nested case-control study was based on RERF Research Protocol 1-04 and approved by the Human Investigation Committee of Radiation Effects Research Foundation.

Statistical Analyses. The nested case-control design is analyzed using a partial likelihood method analogous to that used for cohort follow-up studies (29), which is, in practice, the same as the conditional binary data likelihood for matched case-control studies (30) except that the subjects (cases and controls) in the study are not completely independent because of the possibility of repeated selection. All factors other than radiation were analyzed using relative risks estimated by a log-linear model. The population attributable fraction was estimated for individual factors that increased the risk for hepatocellular carcinoma in the present study. Population attributable fraction was calculated as $pd \times [(mRR - 1) / mRR]$, where mRR is the multivariate adjusted relative risk for the covariates and pd is the proportion of cases exposed to the risk factor. Statistical interaction between viral infection and BMI was tested by adding the product of the two factors to the log-linear model, which tests departure from a multiplicative relationship. Reported P values and confidence limits are based on Wald statistics. Although radiation exposure could have been adjusted by matching on radiation dose as an additional matching factor in the control selection (31), in addition to assessing effects of lifestyle factors and viral hepatitis, another purpose of the present study was to examine effects of radiation exposure after adjustment for possible confounding and interaction by these factors, so matching on radiation, which prevents analysis of radiation risk, was not desirable; rather, we countermatched on radiation (29, 32). Radiation risk was analyzed by using an excess relative risk model as has been done previously (33).

Results

Characteristics of Study Population. Characteristics of the 224 hepatocellular carcinoma cases and 644 comparison subjects are shown in Table 1. The mean age of the cases was 67.6 years, and 61% were men. Cases and controls were comparable with respect to gender, age, city, time of serum storage, and method of serum storage by design. Virological and biochemical assays were done on 211 case and 640 control sera because 13 case samples and 4 control samples had insufficient stored sera for these assays. Hepatocellular carcinoma

case sera evidenced a higher prevalence of HBV or HCV infection status, higher values of fibrosis markers and ferritin, and lower platelet counts compared with control sera. Greater proportions of hepatocellular carcinoma cases had a history of alcohol consumption of ≥40 g of ethanol per day, were current smokers, were obese, had diabetes mellitus, and received high radiation doses compared with the controls. In addition, hepatocellular carcinoma cases were less likely than controls to be daily coffee drinkers. There were no important differences in characteristics such as gender, age at hepatocellular carcinoma diagnosis, city, or BMI between hepatocellular carcinoma cases excluded because of nonavailability of stored serum and those included in this study.

Risk Factors for Hepatocellular Carcinoma Development. Table 2 shows the results of univariate and multivariate analyses using HBV and HCV infection status, alcohol consumption, smoking habit, coffee drinking, BMI, diabetes mellitus, and radiation dose. Strong association was found between hepatocellular carcinoma and hepatitis virus infection, resulting in unadjusted relative risks of 33.7 [95% confidence interval (95% CI), 12.7-89.6] for HBV+/HCV− status and 64.5 (95% CI, 29.1-143) for HBV−/HCV+ status. As expected, the risk for hepatocellular carcinoma for alcohol consumption was significant, with an unadjusted relative risk of 1.34 (95% CI, 1.12-1.60) per 20 g of ethanol per day using continuous alcohol consumption and 2.66 (95% CI, 1.55-4.55) at ≥40 g of ethanol per day using grouped alcohol consumption. Although the grouped results suggest that a simple log-linear model in continuous alcohol consumption may not be adequate, a quadratic term did not significantly improve the model (data not shown). Current smoking was significantly associated with hepatocellular carcinoma risk, with an unadjusted relative risk of 1.87 (95% CI, 1.14-3.07). Daily coffee drinking was associated with decreased risk for hepatocellular carcinoma, with an unadjusted relative risk of 0.51 (95% CI, 0.29-0.90). The presence of obesity and diabetes mellitus 10 years before diagnosis were statistically associated with increased risk for hepatocellular carcinoma, resulting in unadjusted relative risks of 1.88 (95% CI, 1.13-3.13) and 1.88 (95% CI, 1.01-3.50), respectively. The relative risk for a 1-unit difference in BMI was 1.04 (95% CI, 0.99-1.09). Radiation exposure was marginally significantly associated with increased risk for hepatocellular carcinoma ($P = 0.055$).

The risks for viral infection in multivariate analysis did not meaningfully differ from those obtained in the univariate analysis. Alcohol consumption of ≥40 g of ethanol per day and obesity remained significant risk factors for hepatocellular carcinoma even after adjusting for viral infection status and the other factors, whereas the effects of current smoking and diabetes mellitus became nonsignificant after adjustment. Daily coffee drinking was marginally significantly associated with decreased risk for hepatocellular carcinoma after adjustment for viral infection and the other factors. The adjusted relative risk for a one unit difference in BMI, 1.12 (95% CI, 1.03-1.22), was statistically significant, but a quadratic term was not significant.

Table 3 shows the estimated population attributable fraction based on the multivariate adjusted relative risks in the present study. The proportion of hepatocellular

Table 2. Relative risks of hepatocellular carcinoma for individual factors

Variables	Unadjusted		Multivariate adjusted	
	RR (95% CI)	*P*	RR (95% CI)*	*P*
Etiology (HBV/HCV status)				
HBV−/HCV−	1	—	1	—
HBV+/HCV−	33.7 (12.7-89.6)	<0.001	45.8 (15.2-138)	<0.001
HBV−/HCV+	64.5 (29.1-143)	<0.001	101 (38.7-263)	<0.001
HBV+/HCV+	42.4 (6.2-291)	<0.001	70.7 (8.3-601)	<0.001
Alcohol consumption (g of ethanol per day)				
Never	1	—	1	—
>0 and <20	1.11 (0.69-1.78)	>0.5	1.27 (0.56-2.87)	>0.5
≥20 and <40	1.07 (0.57-1.99)	>0.5	1.02 (0.34-3.05)	>0.5
≥40	2.66 (1.55-4.55)	<0.001	4.36 (1.48-13.0)	0.008
Continuous (per 20-g ethanol per day)	1.34 (1.12-1.60)	<0.001	1.73 (1.19-2.52)	0.004
Smoking habit				
Never	1	—	1	—
Current smoking	1.87 (1.14-3.07)	0.014	2.03 (0.82-4.98)	0.13
Prior smoking	1.80 (0.81-3.99)	0.15	1.12 (0.25-5.07)	>0.5
Coffee drinking				
Never	1	—	—	—
Daily	0.51 (0.29-0.90)	0.016	0.40 (0.16-1.02)	0.055
BMI (kg/m^2) 10 y before diagnosis				
≤19.5	1.24 (0.73-2.11)	0.43	1.31 (0.51-3.34)	>0.5
19.6-21.2	0.97 (0.55-1.70)	>0.5	1.24 (0.43-3.54)	>0.5
21.3-22.9	1	—	1	—
23-25	1.61 (0.96-2.70)	0.074	2.51 (0.99-6.37)	0.053
>25	1.88 (1.13-3.13)	0.016	4.57 (1.85-11.3)	<0.001
Continuous (+1 kg/m^2 difference)	1.04 (0.99-1.09)	0.087	1.12 (1.03-1.22)	0.010
Diabetes 10 y before diagnosis	1.88 (1.01-3.50)	0.047	1.98 (0.63-6.27)	0.24

Abbreviation: RR, relative risk.
*Adjusted for hepatitis virus infection, continuous alcohol consumption, smoking habit, coffee drinking, BMI, diabetes mellitus, and radiation dose to the liver.

Table 3. Estimated population attributable fraction of hepatocellular carcinoma for risk factors in this study population

Variables*	Proportion of cases exposed (%)	Multivariate-adjusted RR	Population attributable fraction (%)
Etiology (HBV/HCV status)			
HBV+/HCV−	13.7	45.8	13.4
HBV−/HCV+	62.6	101	62.0
HBV+/HCV+	2.4	70.7	2.4
Alcohol consumption			
≥40-g ethanol per day	22.6	4.36	17.4
BMI 10 y before diagnosis			
>25 kg/m^2	25.7	4.57	20.1

*Population attributable fraction was estimated only for the significant hepatocellular carcinoma risk factors.

carcinoma cases that is attributable to HBV+/HCV−, HBV−/HCV+, HBV+/HCV+, alcohol consumption of ≥40 g of ethanol per day, and obesity were 13.4%, 62.0%, 2.4%, 17.4%, and 20.1%, respectively. These values are not mutually exclusive because some cases were exposed to more than one risk factor.

Analyses with Adjustment for Variables Associated with Severity of Liver Fibrosis. Table 4 shows results for univariate analyses incorporating biomarkers associated with progression of liver fibrosis, such as hyaluronic acid and type IV collagen of fibrosis markers, platelet count, and ferritin. Large statistically significant differences in the mean values of these variables were observed between hepatocellular carcinoma cases and controls. Figure 1 shows a comparison of multivariate analysis results with or without adjustment for ln(type IV collagen) and platelet count using HBV and HCV infection status, alcohol consumption, smoking habit, coffee drinking, BMI, diabetes mellitus, and radiation dose as adjustment variables. We evaluated type IV collagen and platelet count as surrogate markers associated with severity of liver fibrosis. Hepatocellular carcinoma risk for hepatitis virus infection status after adjusting for liver fibrosis meaningfully decreased compared with the results indicated in the previous multivariate analysis, with relative risks of 20.8 (95% CI, 4.8-90.3) and 37.8 (95% CI, 12.4-115) for HBV+/HCV− status and HBV−/HCV+ status, respectively (Fig. 1A). Effects of ≥40 g of ethanol per day and daily coffee drinking decreased and disappeared, respectively, so that adjustment for liver fibrosis decreased the effect of these factors on risk for hepatocellular carcinoma. Current smoking became marginally significantly associated with increased risk for hepatocellular carcinoma after adjusting for liver fibrosis. Obesity remained a significant risk factor independent of adjustment for severity of liver fibrosis, and the relative risk for diabetes mellitus did not meaningfully differ from that without such adjustment (Fig. 1B).

Interaction between Hepatitis Virus Infection Status and Increase of BMI. Table 5 shows the joint effects of hepatitis virus infection status and BMI, with adjustment for alcohol consumption, smoking habit, coffee drinking, diabetes mellitus, and radiation dose. Although being obese was clearly a risk factor for hepatocellular carcinoma subjects with adjustment for viral factors, it was not a significant risk factor in those with HBV−/HCV− status. However, despite the appearance of a trend with BMI, only 15 hepatocellular carcinoma cases were identified among HBV−/HCV− individuals with obesity. Among hepatocellular carcinoma subjects with HBV−/HCV+ status, the relative risk increased dramatically with increasing BMI. Linear (P = 0.003) and quadratic (P = 0.013) terms in continuous BMI were

Table 4. Relative risks of hepatocellular carcinoma for variables associated with severity of liver fibrosis: unadjusted relative risk and 95% CI

Variables	Hepatocellular carcinoma cases/controls	Unadjusted	
		RR (95% CI)	P
Liver fibrosis markers	211/640		
Hyaluronic acid (+per 10 ng/mL)		1.10 (1.08-1.12)	<0.001
ln(hyaluronic acid) (+per 1 unit)		5.43 (4.04-7.30)	<0.001
Type IV collagen (+per 10 ng/mL)		1.14 (1.10-1.17)	<0.001
ln(type IV collagen) (+per 1 unit)		80.9 (35.8-183)	<0.001
Platelet count	151/448		
+Per 10^4/μL		0.75 (0.71-0.80)	<0.001
≥25.0 (×10^4/μL)	4/133	1	
20.0-24.9 (×10^4/μL)	19/163	4.5 (1.3-1.6)	0.02
15.0-19.9 (×10^4/μL)	26/105	11.8 (3.2-43)	<0.001
10.0-14.9 (×10^4/μL)	52/42	61 (16-232)	<0.001
<10.0 (×10^4/μL)	50/5	822 (125-5400)	<0.001
Ferritin	206/635		
+ Per 10 ng/mL		1.03 (1.02-1.04)	<0.001
ln(ferritin) (+per 1 unit)		1.51 (1.25-1.82)	<0.001

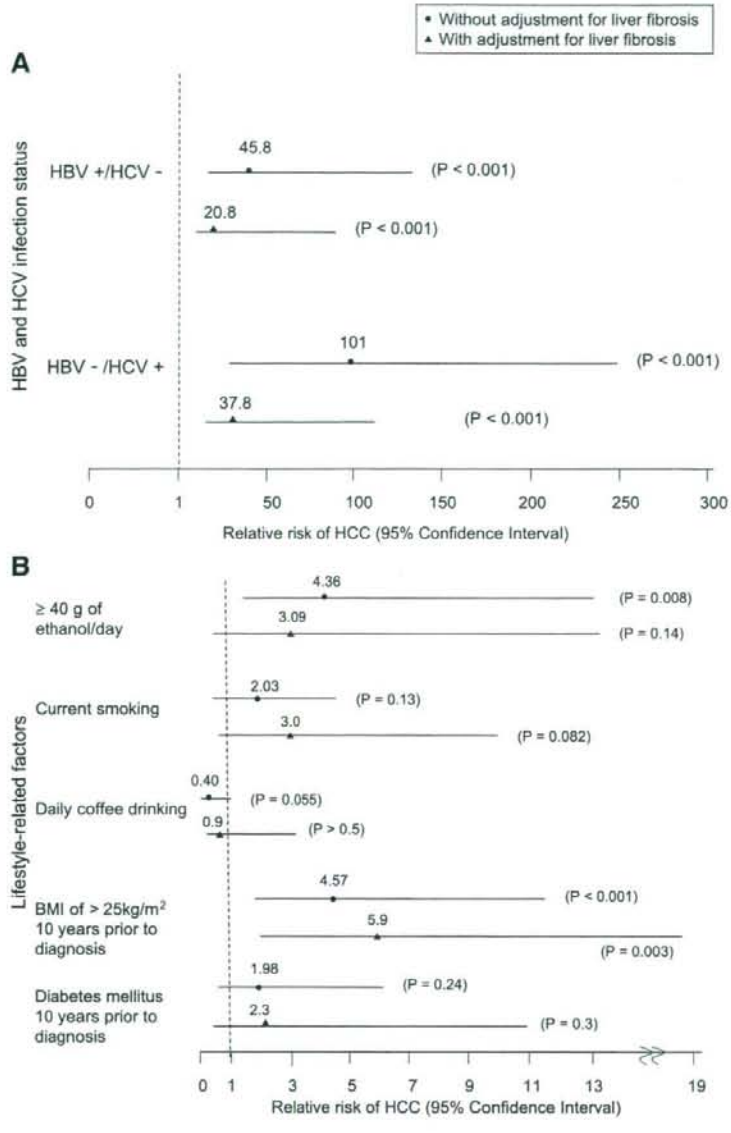

Figure 1. Multivariate relative risk for hepatocellular carcinoma for individual risk factors, with and without adjustment for variables associated with severity of liver fibrosis. Each relative risk was analyzed with and without adjustment for ln(type IV collagen) and platelet count, using HBV and HCV infection status, continuous alcohol consumption, smoking habit, coffee drinking, BMI, diabetes mellitus, and radiation dose as adjustment variables. **A.** HBV and HCV infection status. **B.** Lifestyle-related factors. *HCC*, hepatocellular carcinoma.

significant among HBV−/HCV+ individuals. Among hepatocellular carcinoma subjects with HBV+/HCV− status, the relative risk for hepatocellular carcinoma did not show evidence of an increase with increased BMI, although the examination of a joint effect of HBV infection and BMI was based on only one hepatocellular carcinoma case out of three subjects who were HBV+/HCV− and obese. The reason for the relatively small unadjusted relative risk for obesity (Table 2) might have been due to the small number of cases and controls with HBV+/HCV− status, which apparently offset the increase observed in HBV−/HCV+ status individuals.

Discussion

This nested case-control study indicated that HBV and HCV infection, alcohol consumption of ≥40 g of ethanol per day, and obesity 10 years before hepatocellular carcinoma diagnosis were independent risk factors for hepatocellular carcinoma, and that obesity as well as hepatitis virus infection remained independent risk factors for hepatocellular carcinoma after taking into account the severity of liver fibrosis. Furthermore, significant multiplicative interaction in hepatocellular carcinoma risk between viral etiology and increased BMI was observed in HCV-infected individuals. The

population attributable fraction of 62.0% for hepatocellular carcinoma cases with HCV infection was highest, and hepatocellular carcinoma cases with HBV infection, alcohol consumption of ≥40 g of ethanol per day, or obesity had population attributable fractions in the range of 13.4% to 20.1%. These are only approximate estimates of the potential for reducing hepatocellular carcinoma occurrence, as we do not know what effect removal of one risk factor would have on the distribution of the other risk factors.

Multivariate analysis after adjusting for severity of liver fibrosis indicated that hepatocellular carcinoma risk for HBV and HCV infections significantly decreased, which is consistent with the existing notion that hepatocellular carcinoma risk increases with progression from chronic hepatitis B and C to liver cirrhosis. A large-scale meta-analysis (34) and a case-control study (35) showed a combined effect of HBV and HCV infections on hepatocellular carcinoma risk, whereas our study did not detect similar effects among those with HBV+/HCV+ status. This difference may be partly attributable to the extremely limited number of coinfected subjects with HBV and HCV among our study population. It may be also partly because most past epidemiologic studies have defined chronic HCV infection by either anti-HCV antibody positivity or by HCV RNA positivity in serum (34, 35).

Several epidemiologic studies and clinical trials revealed an association between obesity and hepatocellular carcinoma risk (9-12), but few population-based cohort studies have been conducted with precise adjustment for HBV and HCV infection status, the major risk factors for hepatocellular carcinoma. Obesity was recently found to be one of the etiologic factors for nonalcoholic steatohepatitis, which is considered a non-B, non-C liver disease, and it has been shown to be a risk factor for hepatocellular carcinoma (12, 16). Although many clinical studies showed that, among chronic hepatitis C patients, obesity was associated with progression of inflammation, insulin resistance, hepatic steatosis, and liver fibrosis (17, 36), a study by Nair et al. (12) reported that obesity was not an independent risk factor for hepatocellular carcinoma among liver cirrhosis patients with HBV and HCV. On the other hand, a recent Western cohort study showed that being overweight (BMI, 25 to <30 kg/m^2) or obese (BMI, ≥30 kg/m^2) was an independent risk factor for hepatocellular carcinoma (37).

In the present study, we adjusted for potentially confounding factors including hepatitis virus infection and also found that being obese 10 years before hepatocellular carcinoma diagnosis was associated with a 4.57-fold increase in hepatocellular carcinoma risk. Furthermore, we observed a statistically significant, positive, multiplicative interaction between HCV infection and increased BMI on the risk for hepatocellular carcinoma, which indicates decisively that the joint effect of the two factors is greater than additive.

Obesity contributes to a high rate of visceral fat storage, accelerating production of tumor necrosis factor-α, interleukin 6, resistin, and leptin, and decreasing production of adiponectin (16). These cytokines presumably foster insulin resistance (16), cause hepatic steatosis and oxidative stress, and eventually promote hepatocellular carcinoma occurrence. A large number of studies pointed out association between progression of liver fibrosis and insulin resistance or hepatic steatosis (15-17), but authenticity of any connection is now being questioned (8, 36). Interestingly, in this study, obesity remained an independent risk factor for hepatocellular carcinoma even after adjusting for all confounding factors including severity of liver fibrosis. The following are the possible reasons why obesity increases hepatocellular carcinoma risk irrespective of severity of liver fibrosis: Several animal experiments showed that liver tumors were not always accompanied by advanced fibrosis among a variety of genetically engineered mouse models with steatohepatitis (38), and some reports indicated several nonalcoholic steatohepatitis–derived human cancer cases without significant liver fibrosis (39). The findings suggest that significant liver fibrosis is not essential for the carcinogenic process, but that steatohepatitis itself is a state conferring a risk for high carcinogenicity. With regard to the proven relationship between obesity and such malignant tumors as colon, breast, and ovarian cancers (10), the cell proliferation activity of insulin due to hyperinsulinemia is believed to play a role in a common carcinogenic mechanism (5).

It is well documented that obesity induces insulin resistance, with a tendency to cause diabetes mellitus. In the case of hepatic cirrhosis accompanied by highly advanced liver fibrosis, glucose intolerance tends to lead to diabetes mellitus. A recent animal experiment showed that HCV contributed to progression of insulin resistance, resulting in diabetes mellitus (40). The present study failed to show that diabetes mellitus 10 years before hepatocellular carcinoma diagnosis was an independent risk factor for hepatocellular carcinoma, but an adjustment for all factors, except alcohol consumption and BMI, brought about a 30% increase in the effect of diabetes on hepatocellular carcinoma risk (data not shown). Such findings suggest a relationship between diabetes mellitus and alcohol consumption, as well as BMI. Therefore, by taking into account the proven association between alcohol consumption, obesity, and increased risk for hepatocellular carcinoma, our results will not likely refute an association between diabetes mellitus and hepatocellular carcinoma risk.

A large number of epidemiologic studies showed that heavy alcohol consumption was an independent risk factor for hepatocellular carcinoma and that there was

Table 5. Interaction between hepatitis virus infection status and increase of BMI on hepatocellular carcinoma risk (joint hepatitis virus/BMI)

Viral etiology	BMI (kg/m^2)	RR* (95% CI)†	Likelihood ratio P†
HBV−/HCV−	+1	1.05 (0.95-1.17)	0.33
HBV+/HCV−	+1	0.89 (0.64-1.23)	0.50
HBV−/HCV+	+1	1.39 (1.11-1.83)	0.003‡
HBV+/HCV+	+1	—§	—§

*Adjusted for continuous alcohol consumption, smoking habit, coffee drinking, diabetes mellitus, and radiation dose to the liver.
†Likelihood bounds and P values for relative risks estimated separately within each BMI/hepatitis virus category.
‡A quadratic term was also significant for HBV−/HCV+ individuals (P = 0.013). However, only the relative risk for the linear model in continuous BMI is shown because it is not possible to express the risk as a single value with a two-parameter linear-quadratic model.
§Neither could the joint effect of obesity and simultaneous HBV+/HCV+ status be estimated because of small numbers of jointly affected cases and controls.

correlation between increased risk for hepatocellular carcinoma and amount of alcohol consumed (3, 9, 13, 14). In addition, in some case-control studies of hepatocellular carcinoma risk, synergistic interactions between alcohol consumption and hepatitis virus infection, or between obesity and diabetes mellitus, have been observed (9, 13, 14). In the present study, after adjusting for other factors such as hepatitis virus infection and BMI, alcohol consumption of ≥40 g of ethanol produced a 4.36-fold increase in hepatocellular carcinoma risk. A few recent case-control studies suggested that ethanol consumption of <50 to 60 g/d (41, 42) or alcohol exposure <1,500 gram-years (9) had protective effects on the progression of liver fibrosis and risk for developing hepatocellular carcinoma. Reasons for such discrepancy between our result and former reports are unclear, but factors such as gender, age, race (43), hereditary predisposition, and etiology of liver disease presumably affect the severity of alcohol-related liver diseases. Our study also showed that effects of alcohol consumption of ≥40 g of ethanol per day on hepatocellular carcinoma risk were reduced after adjusting for all confounding factors including severity of liver fibrosis. The finding suggests that alcohol consumption may contribute to hepatic carcinogenesis by enhancing oxidative stress and aggravating liver fibrosis.

As a result of recent assessments by the IARC, hepatocellular carcinoma has been positioned as a smoking-related malignant disease (44). However, it has yet to be determined whether smoking itself has direct hepatic carcinogenic effects or whether smoking contributes to hepatic carcinogenesis by way of progression of liver fibrosis. A case-control study showed that 4-aminobiphenyl DNA adducts contained in tobacco smoke are a liver carcinogen (45). In the present study, we adjusted for potential confounding factors including hepatitis virus infection and failed to detect significant smoking effects on hepatocellular carcinoma risk; however, a multivariate analysis that excluded hepatitis virus infection showed significant effects of smoking (data not shown). With adjustment for all factors including severity of liver fibrosis, effects of smoking on hepatocellular carcinoma risk were found to be marginally significant. These findings suggest the possibility that smoking, in conjunction with hepatitis virus infection, further enhances the risk for hepatocellular carcinoma and might directly contribute to the mechanism of liver carcinogenesis.

Several epidemiologic studies indicated the involvement of coffee in decreased alanine aminotransferase activity and γ-glutamyltransferase level, suppression of progression to liver cirrhosis, and inhibited development of hepatocellular carcinoma (18, 19). Such oxidation inhibitors as caffeine, coffee diterpenes, and chlorogenic acid are among candidate substances in coffee that potentially reduce the risk for hepatocellular carcinoma, and several animal experiments have shown that such substances have direct inhibitory effects on hepatic carcinogenesis (46). Adjusting for all potential confounding factors including hepatitis virus infection rendered the effects of coffee drinking on hepatocellular carcinoma risk marginally significant, whereas adjusting for all factors, except hepatitis virus infection, revealed significant effects of coffee drinking (data not shown). Furthermore, adjusting for all factors including severity of liver fibrosis erased the effects of coffee drinking on hepatocellular carcinoma risk. These findings suggest that coffee drinking may somehow suppress liver fibrosis and thereby indirectly reduce hepatocellular carcinoma risk.

The main strengths of our study are its prospective cohort-based, nested case-control design, which minimized selection bias and provided for the use of stored sera and a wealth of epidemiologic information obtained before hepatocellular carcinoma diagnosis. Indeed, the distributions of HBV and HCV infection status among hepatocellular carcinoma cases and controls and mean age at diagnosis among hepatocellular carcinoma cases were similar to those in previous reports on Japanese populations (2, 4). Another major strength of our study is that it incorporated, in a strict and in-depth manner, HBV and HCV infection status and showed the interrelationship between these and numerous other epidemiologic factors. It is difficult and expensive to perform full cohort serum analyses, whereas the nested case-control design used here can provide substantial reductions in cost and effort with little loss of statistical efficiency.

The main limitation of our study is that the severity of liver fibrosis could not be classified into fibrosis stage of F0 to F4 based on liver specimens. We used platelet counts and type IV collagen concentrations as surrogate, but independent, markers of liver fibrosis. Previous reports showed a strong correlation between platelet count and fibrosis stage in the presence of chronic hepatitis C (47) and a close association between levels of type IV collagen, a basic component of the hepatic basal membrane, and severity of liver fibrosis. Another limitation of our study is the usage of sera that had been stored for long periods of time. Proteins and HCV RNA trend to degrade during prolonged storage of either frozen or freeze-dried sera. However, we minimized this degradative effect by the selection of matched controls relative to time and method of serum storage. Furthermore, we have previously shown that the freeze-dried sera are interchangeable with frozen sera in serologic and molecular biological detection of HBV and HCV (22, 25). Finally, some hepatocellular carcinoma cases had to be excluded because of nonavailability of stored sera. We did not detect any differences between included and excluded cases in terms of demographic variables or BMI.

In conclusion, HBV and HCV infection and obesity were independent risk factors for hepatocellular carcinoma, even after taking into account the severity of liver fibrosis. Moreover, the combination of HCV infection and increased BMI exerted a synergistic effect on the risk for hepatocellular carcinoma. Alcohol consumption of ≥40 g of ethanol per day was also an independent risk factor for hepatocellular carcinoma, likely contributing to the development of hepatocellular carcinoma through liver fibrosis. The radiation effect on hepatocellular carcinoma risk was shown to be marginally significant in univariate analysis; whether the radiation effect is confounded with other factors will be closely examined in a separate report. A precise understanding of the mechanism by which obesity contributes to development of hepatocellular carcinoma should lead to better therapeutic strategies, public health policies, and cost-effectiveness.

Acknowledgments

We thank Naomi Masunari and Sachiko Teranishi for the collection and processing of the data; all members of division of clinical laboratories for their excellent assistance in experiments; and Michiko Yamada, Yoshimi Tatsukawa, and Kyoji Furukawa for helpful discussion. The Radiation Effects Research Foundation, Hiroshima and Nagasaki, Japan, is a private, nonprofit foundation funded by the Japanese Ministry of Health, Labour and Welfare and the U.S. Department of Energy, the latter through the National Academy of Sciences.

References

1. Yu MC, Yuan JM. Environmental factors and risk for hepatocellular carcinoma. Gastroenterology 2004;127:S72–8.
2. Kiyosawa K, Umemura T, Ichijo T, et al. Hepatocellular carcinoma: recent trends in Japan. Gastroenterology 2004;127:S17–26.
3. Aizawa Y, Shibamoto Y, Takagi I, Zeniya M, Toda G. Analysis of factors affecting the appearance of hepatocellular carcinoma in patients with chronic hepatitis C. A long term follow-up study after histologic diagnosis. Cancer 2000;89:53–9.
4. Ohishi W, Kitamoto M, Aikata H, et al. Impact of aging on the development of hepatocellular carcinoma in patients with hepatitis C virus infection in Japan. Scand J Gastroenterol 2003;38:894–900.
5. Gupta K, Krishnaswamy G, Karnad A, Peiris AN. Insulin: a novel factor in carcinogenesis. Am J Med Sci 2002;323:140–5.
6. El-Serag HB, Tran T, Everhart JE. Diabetes increases the risk of chronic liver disease and hepatocellular carcinoma. Gastroenterology 2004;126:460–8.
7. Inoue M, Iwasaki M, Otani T, Sasazuki S, Noda M, Tsugane S. Diabetes mellitus and the risk of cancer: results from a large-scale population-based cohort study in Japan. Arch Intern Med 2006;166:1871–7.
8. Caldwell SH, Crespo DM, Kang HS, Al-Osaimi AM. Obesity and hepatocellular carcinoma. Gastroenterology 2004;127:S97–103.
9. Marrero JA, Fontana RJ, Fu S, Conjeevaram HS, Su GL, Lok AS. Alcohol, tobacco and obesity are synergistic risk factors for hepatocellular carcinoma. J Hepatol 2005;42:218–24.
10. Calle EE, Rodriguez C, Walker-Thurmond K, Thun MJ. Overweight, obesity, and mortality from cancer in a prospectively studied cohort of U.S. adults. N Engl J Med 2003;348:1625–38.
11. Oh SW, Yoon YS, Shin SA. Effects of excess weight on cancer incidences depending on cancer sites and histologic findings among men: Korea National Health Insurance Corporation Study. J Clin Oncol 2005;23:4742–54.
12. Nair S, Mason A, Eason J, Loss G, Perrillo RP. Is obesity an independent risk factor for hepatocellular carcinoma in cirrhosis? Hepatology 2002;36:150–5.
13. Hassan MM, Hwang LY, Hatten CJ, et al. Risk factors for hepatocellular carcinoma: synergism of alcohol with viral hepatitis and diabetes mellitus. Hepatology 2002;36:1206–13.
14. Yuan JM, Govindarajan S, Arakawa K, Yu MC. Synergism of alcohol, diabetes, and viral hepatitis on the risk of hepatocellular carcinoma in blacks and whites in the U.S. Cancer 2004;101:1009–17.
15. Ferrannini E. Insulin resistance, iron, and the liver. Lancet 2000;355:2181–2.
16. Bugianesi E, McCullough AJ, Marchesini G. Insulin resistance: a metabolic pathway to chronic liver disease. Hepatology 2005;42:987–1000.
17. Hu KQ, Kyulo NL, Esrailian E, et al. Overweight and obesity, hepatic steatosis, and progression of chronic hepatitis C: a retrospective study on a large cohort of patients in the United States. J Hepatol 2004;40:147–54.
18. Inoue M, Yoshimi I, Sobue T, Tsugane S; JPHC Study Group. Influence of coffee drinking on subsequent risk of hepatocellular carcinoma: a prospective study in Japan. J Natl Cancer Inst 2005;97:293–300.
19. Ruhl CE, Everhart JE. Coffee and caffeine consumption reduce the risk of elevated serum alanine aminotransferase activity in the United States. Gastroenterology 2005;128:24–32.
20. Yaginuma K, Kobayashi H, Kobayashi M, Morishima T, Matsuyama K, Koike K. Multiple integration site of hepatitis B virus DNA in hepatocellular carcinoma and chronic active hepatitis tissues from children. J Virol 1987;61:1808–13.
21. Moriya K, Nakagawa K, Santa T, et al. Oxidative stress in the absence of inflammation in a mouse model for hepatitis C virus-associated hepatocarcinogenesis. Cancer Res 2001;61:4365–70.
22. Ohishi W, Fujiwara S, Suzuki G, et al. Feasibility of freeze-dried sera for serological and molecular biological detection of hepatitis B and C viruses. J Clin Microbiol 2006;44:4593–5.
23. Fukuhara T, Sharp GB, Mizuno T, et al. Liver cancer in atomic-bomb survivors: histological characteristics and relationships to radiation and hepatitis B and C viruses. J Radiat Res 2001;42:117–30.
24. Cologne JB, Sharp GB, Neriishi K, Verkasalo PK, Land CE, Nakachi K. Improving the efficiency of nested case-control studies of interaction by selecting controls using counter matching on exposure. Int J Epidemiol 2004;33:485–92.
25. Ohishi W, Fujiwara S, Suzuki G, Chayama K. Validation of the use of freeze-dried sera for the diagnosis of hepatitis B and C virus infections in a longitudinal study cohort. In: Mohan RM, editor. Research Advances in Microbiology 7. Kerala, India: Global Research Network; 2007. p. 1–9.
26. Sharp GB, Lagarde F, Mizuno T, et al. Relationship of hepatocellular carcinoma to soya food consumption: a cohort-based, case-control study in Japan. Int J Cancer 2005;115:290–5.
27. The World Health Organization Western Pacific Region; The International Association for the Study; The International Obesity Task Force. The Asia-Pacific perspective: redefining obesity and its treatment. Sydney, Australia: Health Communications Australia Pty Limited; 2000.
28. Young RW, Kerr GD, editors. Reassessment of the atomic bomb radiation dosimetry for Hiroshima and Nagasaki, Dosimetry System 2002, Report of the Joint US-Japan Working Group. Hiroshima, Japan: Radiation Effects Research Foundation; 2005.
29. Langholz B, Borgan Ø. Counter-matching: a stratified nested case-control sampling method. Biometrika 1985;82:69–79.
30. Breslow NE, Day NE. Statistical methods in cancer research: volume 1—the analysis of case-control studies. Lyon: IARC; 1980.
31. Cologne JB, Shibata Y. Optimal case-control matching in practice. Epidemiology 1995;6:271–5.
32. Cologne J, Langholz B. Selecting controls for assessing interaction in nested case-control studies. J Epidemiol 2003;13:193–202.
33. Cologne JB, Tokuoka S, Beebe GW, Fukuhara T, Mabuchi K. Effects of radiation on incidence of primary liver cancer among atomic bomb survivors. Radiat Res 1999;152:364–73.
34. Donato F, Boffetta P, Puoti M. A meta-analysis of epidemiological studies on the combined effect of hepatitis B and C virus infections in causing hepatocellular carcinoma. Int J Cancer 1998;75:347–54.
35. Kirk GD, Lesi OA, Mendy M, et al. The Gambia Liver Cancer Study: Infection with hepatitis B and C and the risk of hepatocellular carcinoma in West Africa. Hepatology 2004;39:211–9.
36. Perumalswami P, Kleiner DE, Lutchman G, et al. Steatosis and progression of fibrosis in untreated patients with chronic hepatitis C infection. Hepatology 2006;43:780–7.
37. Ioannou GN, Splan MF, Weiss NS, McDonald GB, Beretta L, Lee SP. Incidence and predictors of hepatocellular carcinoma in patients with cirrhosis. Clin Gastroenterol Hepatol 2007;5:938–45.
38. Fan CY, Pan J, Usuda N, Yeldandi AV, Rao MS, Reddy JK. Steatohepatitis, spontaneous peroxisome proliferation and liver tumors in mice lacking peroxisomal fatty acyl-CoA oxidase. Implications for peroxisome proliferator-activated receptor α natural ligand metabolism. J Biol Chem 1998;273:15639–45.
39. Bullock RE, Zaitoun AM, Aithal GP, Ryder SD, Beckingham IJ, Lobo DN. Association of non-alcoholic steatohepatitis without significant fibrosis with hepatocellular carcinoma. J Hepatol 2004;41:685–6.
40. Shintani Y, Fujie H, Miyoshi H, et al. Hepatitis C virus infection and diabetes: direct involvement of the virus in the development of insulin resistance. Gastroenterology 2004;126:840–8.
41. Donato F, Tagger A, Gelatti U, et al. Alcohol and hepatocellular carcinoma: the effect of lifetime intake and hepatitis virus infections in men and women. Am J Epidemiol 2002;155:323–31.
42. Monto A, Patel K, Bostrom A, et al. Risks of a range of alcohol intake on hepatitis C-related fibrosis. Hepatology 2004;39:826–34.
43. Iwahashi K, Matsuo Y, Suwaki H, Nakamura K, Ichikawa Y. CYP2E1 and ALDH2 genotypes and alcohol dependence in Japanese. Alcohol Clin Exp Res 1995;19:564–6.
44. IARC. IARC Monographs on the evaluation of the carcinogenic risks to humans. Volume 83: tobacco smoke and involuntary smoking. Lyon: IARC; 2004.
45. Wang LY, Chen CJ, Zhang YJ, et al. 4-Aminobiphenyl DNA damage in liver tissue of hepatocellular carcinoma patients and controls. Am J Epidemiol 1998;147:315–23.
46. Tanaka T, Nishikawa A, Shima H, et al. Inhibitory effects of chlorogenic acid, reserpine, polyprenoic acid (E-5166), or coffee on hepatocarcinogenesis in rats and hamsters. Basic Life Sci 1990;52:429–40.
47. Pohl A, Behling C, Oliver D, Kilani M, Monson P, Hassanein T. Serum aminotransferase levels and platelet counts as predictors of degree of fibrosis in chronic hepatitis C virus infection. Am J Gastroenterol 2001;96:3142–6.

Published online 3 October 2008

Nucleic Acids Research, 2008, Vol. 36, No. 19 **6295–6308**
doi:10.1093/nar/gkn609

Biochemical analysis of human PIF1 helicase and functions of its N-terminal domain

Yongqing Gu[1,2], Yuji Masuda[1] and Kenji Kamiya[1,*]

[1]Research Institute for Radiation Biology and Medicine, Hiroshima University, Hiroshima 734-8553, Japan and [2]School of Medicine, Shihezi University, Shihezi, Xinjiang 832002, China

Received May 1, 2008; Revised September 8, 2008; Accepted September 9, 2008

ABSTRACT

The evolutionary conserved PIF1 DNA helicase family appears to have largely nonoverlapping cellular functions. To better understand the functions of human PIF1, we investigated biochemical properties of this protein. Analysis of single-stranded (ss) DNA-dependent ATPase activity revealed nonstructural ssDNA to greatly stimulate ATPase activity due to a high affinity for PIF1, even though PIF1 preferentially unwinds forked substrates. This suggests that PIF1 needs a ssDNA region for loading and a forked structure for translocation entrance into a double strand region. Deletion analysis demonstrated novel functions of a unique N-terminal portion, named the PIF1 N-terminal (PINT) domain. When the PINT domain was truncated, apparent affinity for ssDNA and unwinding activity were much reduced, even though the maximum velocity of ATPase activity and K_m value for ATP were not affected. We suggest that the PINT domain contributes to enhancing the interaction with ssDNA through intrinsic binding activity. In addition, we found DNA strand-annealing activity, also residing in the PINT domain. Notably, the unwinding and annealing activities were inhibited by replication protein A. These results suggest that the functions of PIF1 might be restricted with particular situations and DNA structures.

INTRODUCTION

Helicases are ubiquitous enzymes that catalyze the unwinding of DNA duplexes using ATP as their energy source. They therefore play vital roles in nearly all DNA metabolic processes, including DNA replication, recombination and repair. The PIF1 subfamily of 5′–3′ DNA helicases (1–10) belongs to the SFI superfamily, conserved in diverse organisms (11).

In *Saccharomyces cerevisiae* (*Sc*), *Sc*Pif1 was originally identified because of its involvement in recombination of mitochondrial DNA (mtDNA) (12,13). Dysfunction of *Sc*Pif1 leads to mitochondrial genetic instability due to spontaneous oxidative damage (14–16), and induces mtDNA damage (17). *Sc*Pif1p has not only mitochondrial targeting but also nuclear targeting signals and therefore is localized in both the mitochondria and nucleus (18). Nuclear *Sc*Pif1p has multiple functions. When it is overproduced, telomeres become shorter, while they elongate when it is eliminated (18,19). In the absence of nuclear *Sc*Pif1, gross chromosome rearrangement is also increased, and healing of double-stranded broken ends via telomere addition increases ~200- to 1000-fold. These data suggest a negative regulatory role of *Sc*Pif1 in telomere metabolism (18–24). Indeed, *Sc*Pif1 catalytically inhibits telomerase activity *in vitro* (25). Other genetic data suggest that *Sc*Pif1 plays roles in Okazaki fragment processing (26), pausing of replication progression at ribosomal DNA loci (27) and unwinding of hemicatenans (28).

Schizosaccharomyces pombe encodes a PIF1 homolog, Pfh1 (8,10) which is required for cell cycle progression in late *S*-phase and for appropriate responses to DNA damage agents (8,10). It is also implicated in lagging strand DNA processing (7).

Previous biochemical studies of human PIF1 were performed using N-terminal-truncated forms of PIF1, containing only the conserved helicase motifs, located in the C-terminus, since it earlier proved impossible to obtain purified full-length human PIF1 protein (3,4,9). However, we found that the N-terminal region of human PIF1, named here as the PIF1 N-terminal (PINT) domain, is well conserved in the PIF1 family, suggesting a possible functional role. Here, we established a method to purify full-length human PIF1 protein and provided the first evidence that the PINT domain has crucial functions in this enzyme.

MATERIALS AND METHODS

Plasmid construction

The nucleotide sequence of the 5′-end of human PIF1 cDNA was obtained by 5′-rapid amplification of cDNA ends. Then the full-length human *PIF1* cDNA was

*To whom correspondence should be addressed. Tel: +81 82 257 5842; Fax: +81 82 257 5844; Email: kkamiya@hiroshima-u.ac.jp

amplified from a HeLa cDNA library using primers, CATATGCTCTCGGGCATAGAGGCGGCGGCAGG GGAATATGAGGACTCG and TCAGAGGATTGGG TCCATGTT by PCR, then the nucleotide sequences of the clones were verified and submitted to the database with the accession number, EU084033. The entire coding region with a histidine tag at the N-terminus was inserted into the pET20b(+) vector to yield pET20b-PIF1. The truncated forms, $PIF^{167-641}$ and PIF^{1-180} consisting of the numbered amino acid residues were also cloned into pET20b(+) and pET15b, respectively, to produce his-tagged fusion proteins. The structures of the resultant plasmids, pET20b-PIF1, pET20b-$PIF^{167-641}$ and pET15b-PIF^{1-180}, are shown in Supplementary Figure S1. In this article, $PIF^{167-641}$ and PIF^{1-180} are referred to as C-terminal region of PIF1 (PIF1C) and N-terminal region of PIF1 (PIF1N), respectively.

Protein purification

RPA was purified as described (29) from over producing *Escherichia coli* cells (30). PIF1 and its deletion derivatives were purified as his-tagged fusion proteins at the N-termini. During all the purification steps, induced proteins were monitored by SDS–PAGE followed by staining with Coomassie Brilliant Blue R-250, or western blotting using Penta-His antibody (#34660, QIAGEN, Tokyo, Japan) or anti-PIF1 antibodies. Protein concentrations were determined by Bio-Rad protein assay using BSA (Bio-Rad, Tokyo, Japan) as the standard.

His-tagged full-length PIF1 and PIF1C were purified from overexpressing *E. coli* cells, BL21 (DE3) (31). The strain harboring a plasmid pMStRNA1, in which tRNAs for rare codons were cloned into a R6K derived kanamycin resistant plasmid (32), and pET20b-PIF1 was grown in 3 l of LB supplemented with ampicillin (250 μg/ml) and kanamycine (30 μg/ml) at 15°C, with aeration until the culture reached an A_{600} value of 0.6. Isopropyl β-D-thiogalactopyranoside (IPTG) was added to 0.2 mM, and the incubation was continued for 14 h. The resultant cell paste (9 g) was resuspended in 18 ml of buffer I (50 mM HEPES NaOH pH 7.5, 0.1 mM EDTA, 10 mM β-mercaptoethanol, 1 M NaCl) and frozen in liquid nitrogen. The cells were thawed in ice water and lyzed by addition of 3 ml buffer I containing 100 mM spermidine and 4 mg/ml lysozyme. After incubation on ice for 30 min, heating in a 37°C water bath for 2 min and further incubation on ice for 30 min, the lyzate was clarified by centrifugation twice at 85 000*g* for 30 min at 4°C. Subsequent column chromatography was carried out at 4°C using a fast protein liquid chromatography (FPLC) system (GE Healthcare, Tokyo, Japan). After adding imidazole to 50 mM, the lyzate was applied at 0.2 ml/min to a 1-ml HiTrap chelating column (GE Healthcare), which had been treated with 0.1 M $NiSO_4$ and then equilibrated with buffer A (50 mM HEPES NaOH pH 7.5, 10% glycerol, 10 mM β-mercaptoethanol, 1 M NaCl) containing 50 mM imidazole. The column was washed with 10 ml of equilibration buffer at 0.2 ml/min and his-tagged PIF1 was eluted with 10 ml of buffer A containing 100 mM imidazole. Fractions eluted with 100 mM imidazole were pooled and diluted to 50 mM imidazole with buffer A, then loaded again onto a 1-ml HiTrap chelating column at 0.2 ml/min. The column was washed, and PIF1 was eluted with buffer A containing 300 mM imidazole, then loaded at 0.1 ml/min onto a Superdex 200 10/300 GL column (GE Healthcare) equilibrated with buffer A. PIF1 peak fractions were pooled, frozen in liquid nitrogen, and stored at −80°C. His-tagged PIF1C was purified under the same conditions as described for his-tagged PIF1.

His-tagged human PIF1N was purified from overexpressing *E. coli* cells, Rosetta 2 (DE3) (Novagen, Tokyo, Japan). The strain harboring pET15-PIF1N was grown in 3 l of LB supplemented with ampicillin (250 μg/ml) and chloramphenicol (30 μg/ml) at 15°C with aeration until the culture reached an A_{600} value of 0.6. IPTG was added to 0.2 mM, the incubation was continued for 14 h, and the cells were lyzated as described. After adding imidazole to 50 mM, the lyzate was applied at 0.2 ml/min to a 1-ml HiTrap chelating column, which had been treated with 0.1 M $NiSO_4$ and then equilibrated with buffer A containing 50 mM imidazole. The column was washed with 10 ml of equilibration buffer at 0.2 ml/min and then with 10 ml of buffer A containing 100 mM imidazole. His-tagged PIF1N was eluted with 10 ml of 300 mM imidazole in buffer A. Fractions containing PIF1N were pooled, diluted with buffer B (50 mM HEPES NaOH pH7.5, 10 mM β-mercaptoethanol) to 100 mM of NaCl, and applied at 0.5 ml/min to a 1-ml HiTrap SP HP column (GE Healthcare) equilibrated with buffer B containing 100 mM NaCl. The column was washed with 10 ml of equilibration buffer at 0.1 ml/min, and the PIF1N was eluted with 20 ml of a linear gradient of 100–1000 mM NaCl in buffer B. Fractions containing PIF1N were pooled, frozen in liquid nitrogen and stored at −80°C.

Antibodies

To obtain polyclonal antibodies against PIF1, truncated his-tagged PIF1 proteins (1–180 and 338–641 amino acids) were expressed in Rosetta 2 (DE3), purified and used to immunize rabbits.

DNA substrates

The oligonucleotides employed for the preparation of DNA substrates are listed in Table 1. Oligonucleotides were 5′-end labeled using [γ-^{32}P]ATP (GE Healthcare) and polynucleotide kinase (New England BioLabs, Tokyo, Japan). The schematic structures of substrates are shown in figures, and the labeled oligonucleotides are indicated with asterisks. Annealing reaction mixtures (30 μl) containing the 5′-^{32}P-labeled oligonucleotides at 1 μM, all unlabeled oligonucleotides at 3 μM, 10 mM Tris–HCl (pH 7.5), 7 mM $MgCl_2$ and 200 mM NaCl were heated at 95°C for 10 min, transferred directly to 65°C and held at that temperature for 1 h, slow-cooled to 25°C over a period of 2 h and held at that temperature for 30 min and then cooled to 4°C. Substrates were then purified by electrophoresis through 15–25% polyacrylamide using 0.5× TBE (33) as the electrophoresis buffer. Substrates were eluted from the gel by crushing the gel

slice in TE buffer and incubating overnight at 4°C. The slurry was then filtered through Micro Bio-Spin (Bio-Rad) columns, and the DNA was recovered by ethanol precipitation and resuspended in TE buffer.

ATPase assays

ATPase activity was measured in a standard reaction mixture (20 µl) containing 50 mM Tris–HCl (pH 8.0), 2 mM DTT, 1.2 mM $MgCl_2$, 0.25 mg/ml BSA, 2 mM [γ-^{32}P]ATP, indicated DNA and 1 µl of protein sample diluted with buffer D (50 mM Tris-HCl pH8.0, 1 M NaCl, 2 mM DTT, 10% glycerol, 0.1 mg/ml BSA) to obtain indicated final concentrations. After preincubation for 30 s at 30°C, reactions were initiated by the addition of PIF1 proteins and further incubated for 10 min. After the reaction was stopped with 4 µl of 20 mM EDTA (pH 8.0), an aliquot (2 µl) was spotted onto a polyethyleneimine-cellulose plate (Merck, Tokyo, Japan) and developed in 0.3 M LiCl/0.9 M formic acid. The products were analyzed using a Bio-Imaging Analyzer BAS2000 (Fuji Photo Film Co., Ltd., Tokyo, Japan). The extents of ATP hydrolysis were measured with reference to the relative ratios of radioactivity of inorganic phosphate to uncleaved ATP.

Kinetic assays to determine K_m values for ATP were performed for 10 min in 20 µl reaction mixtures using 14 nM of PIF1 and PIF1C with 3.8 µM and 150 µM (in nucleotides) of M13 mp7 single-stranded (ss) DNA, respectively. Concentrations of ATP ranged from 25 to 400 µM. K_m values were evaluated from the plot of the initial velocity versus the ATP concentration using a hyperbolic curve-fitting program with correlation coefficients (R^2) >0.99.

DNA helicase assays

DNA helicase activity was measured under ATPase assay conditions (20 µl) with the indicated DNA substrate (0.35 nM) and 1 µl of protein sample diluted with buffer D to obtain the indicated final concentrations. After preincubation for 30 s at 30°C, reactions were initiated by the addition of PIF1 proteins and incubated for 10 min at 30°C. Helicase reactions were terminated with 10 µl of stop solution (150 mM EDTA, 30% glycerol, 2% SDS, 0.1% bromophenol blue). In kinetic experiments, a 160-µl reaction mixture was incubated at 30°C and 10-µl aliquots were withdrawn at the indicated times. The reaction products were subjected to electrophoresis through 15–25% polyacrylamide gels in Tris–glycine buffer (33). The gels were dried on DE81 paper (Whatman, Tokyo, Japan) and autoradiographed. DNA products were quantified using a Bio-Imaging Analyzer.

Electrophoretic mobility shift assays

Oligonucleotides were labeled with polynucleotide kinase (New England BioLabs) and [γ-^{32}P]ATP. Assays of DNA binding were performed with a modification of a method described previously (34). The reactions (20 µl) were carried out under ATPase assay conditions, sometimes omitting $MgCl_2$ or ATP, with 25 pM oligonucleotides and 1 µl of protein sample diluted with buffer D to obtain the indicated final concentrations. Incubation was carried out on ice for 10 min followed by loading on prerunning 5% polyacrylamide gels (79:1 acrylamide/*bis*-acrylamide). The electrophoresis buffer contained 6 mM Tris–HCl (pH 8.0), 5 mM sodium acetate and 1 mM EDTA, and the gels were subjected to a constant voltage of 8 V/cm for 100 min at 4°C. Following gel electrophoresis, the products were analyzed as described for the helicase assay. For quantification, fractions of free DNA were measured, and the binding fractions were determined by subtraction from the amount of the free DNA at 0 nM of the protein (35).

For RPA binding experiments, the reactions (20 µl) were carried out under the ATPase assay conditions, sometimes omitting ATP. The substrate 3F:4L (0.35 nM) was incubated, directly or after heating at 100°C for 5 min, with 1 µl of RPA sample diluted with buffer (50 mM HEPES NaOH pH 7.5, 250 mM NaCl, 10 mM β-mercaptoethanol, 10% glycerol) to obtain indicated final concentrations. Incubation was carried out on ice for 10 min, and the products were analyzed as in the PIF1 binding experiments.

DNA strand annealing assays

Strand annealing reactions (20 µl) were carried out under the ATPase assay conditions, but in the presence of the indicated concentrations of ATP, with the 5′-end labeled substrate DNA for helicase assay (0.35 nM), which had been boiled at 100°C for 5 min and quickly chilled on ice before adding to the reaction mixture, and 1 µl of protein sample diluted with buffer D to obtain the indicated final concentrations. After preincubation for 30 s at 30°C, reactions were initiated by the addition of PIF1 proteins, with incubation for 10 min at 30°C. After terminating the reactions with 10 µl of stop solution, the products were analyzed as described for the helicase assay. Kinetic experiments were also carried out as described for the helicase assay.

RESULTS

Purification of PIF1 protein and its deletion derivatives

Previously, biochemical studies of human PIF1 were performed using N-terminal-truncated forms of PIF1 containing only the conserved helicase motifs, located in the C-terminus (Supplementary Figure S2A). However, we found that the PINT domain is well conserved in the PIF1 family (Supplementary Figure S2B), suggesting that it plays a functional role. To examine biochemical activity, we established a procedure to purify full-length PIF1 with a 6× histidine tag at the N-terminus at quantities sufficient for detailed biochemical studies from overproducing *E. coli* cells (Supplementary Figure S2C). We also purified a C-terminal truncated form (PIF1N) and a N-terminal truncated form (PIF1C) (Supplementary Figure S2A) to address biochemical functions of individual domains. PIF1C and PIF1N consist of only the seven helicase motifs and only the PINT domain, respectively (Supplementary Figure S2A and Materials and methods section). Elution profiles from gel filtration chromatography

suggested PIF1 and PIF1C to be monomers (data not shown) as described in yeast homologs (1,5,7). The purified proteins were analyzed by SDS–PAGE followed by CBB staining and western blotting, showing PIF1, PIF1C and PIF1N to have molecular sizes of 71, 54 and 22 kDa, respectively (Supplementary Figure S2C).

Unwinding activities of PIF1 and PIF1C, a mutant lacking PINT domain but containing the helicase domain

We first measured DNA helicase activity of the purified proteins using the indicated DNA substrate (Figure 1A). When 5′ overhang (1F:2S) and 3′ overhang (1R:2S) DNA were used as substrates, we detected helicase activity only on the 5′-overhang substrate, consistent with previous reports (3,9), although the activity was very low (Figure 1B). In the titration experiment, activity was only detected clearly at the maximum concentration of the purified sample (Figure 1B). Since yeast PIF1 homologs preferentially unwind forked structures (1,5,7), we tested a forked substrate (Figure 1C). The titration experiment demonstrated that human PIF1 efficiently unwound the forked substrate with about 10 times higher activity than that for the 5′-overhang substrate (Figure 1C), suggesting that the property was conserved in evolution. Time course experiments using the forked substrate demonstrated that PIF1 could unwind up to 50% of the substrate in a 15 min reaction, although longer incubation did not increase the products (Figure 1D).

To compare the unwinding activity of PIF1C, titration experiments were performed with the forked substrate. We found that PIF1C exhibited helicase activity, but it required more than 100 times more protein to obtain equivalent activity to that of PIF1 (Figure 1C). As a control, we showed that PINT domain itself could not unwind the substrate (Figure 1C). These results suggested that the function of the PINT domain could be enhancement of the unwinding activity of the helicase domain.

Nonstructural ssDNA, but not forked-structural DNA, preferentially stimulates ATPase activity of PIF1

DNA helicases are enzymes with an associated DNA-dependent ATPase activity. They are presumed to use the hydrolysis of ATP to translocate to ssDNA and to subsequently break the hydrogen bonds of duplex DNA. Characterization of ATPase activity could provide important information as a helicase. To analyze ssDNA dependent ATPase activity of PIF1, titration of M13 mp7 ssDNA was performed in reactions with optimal concentrations of ATP and $MgCl_2$ (Figure 2A). The result showed that the ATPase activity was increased depending on the concentrations of ssDNA and reached a plateau between 3 and 50 μM (in nucleotide equivalents) of ssDNA (Figure 2A). The maximum rate of ATP hydrolysis was calculated to be about 1 000 min^{-1}, which was equivalent to 5000 min^{-1} at 37°C of *Sc*Pif1 (5) and 4000 min^{-1} at 30°C of the fission yeast homolog, Pfh1 (7), which have been determined under reaction conditions with nearly saturated concentrations of ssDNA.

To describe precisely the concentration of ssDNA required for ATPase activity, a kinetic parameter,

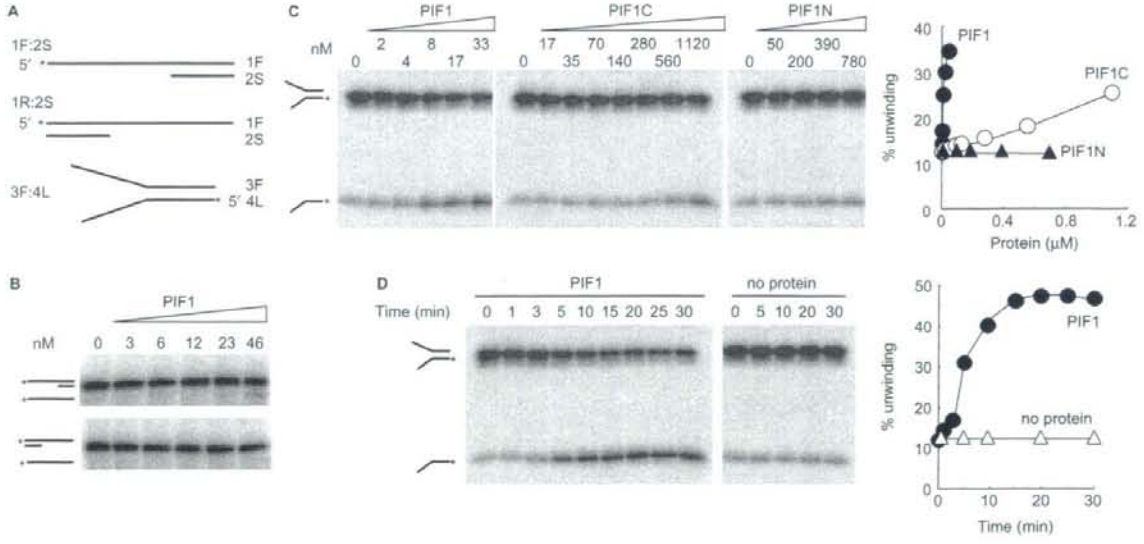

Figure 1. Helicase activity of PIF1. **(A)** Schematic structures of the DNA substrates. The asterisks indicate ^{32}P-labeled 5′ phosphate. **(B)** Helicase activity of PIF1. Increasing levels of PIF1 were incubated with substrates (0.35 nM) with the 5′overhang, 1F:2S (upper panel), or 3′ overhang, 1R:2S (lower panel) under standard reaction mixtures at 30°C for 10 min. Reaction products were separated on a 15–25% polyacrylamide gel. **(C)** Helicase activity of PIF1, PIF1N and PIF1C proteins. The forked structure partial duplex DNA substrate, 3F:4L (0.35 nM), was incubated with the indicated concentrations of PIF1, PIF1N and PIF1C under standard reaction conditions at 30°C for 10 min. The quantified data are shown graphically. The errors in the experiments were <10%. **(D)** Time course of unwinding reactions with PIF1. The forked structure partial duplex DNA substrate, 3F:4L (0.35 nM), was incubated at 30°C for the indicated time under standard reaction conditions with PIF1 (33 nM). The quantified data are shown graphically. The errors in the experiments were <10%.

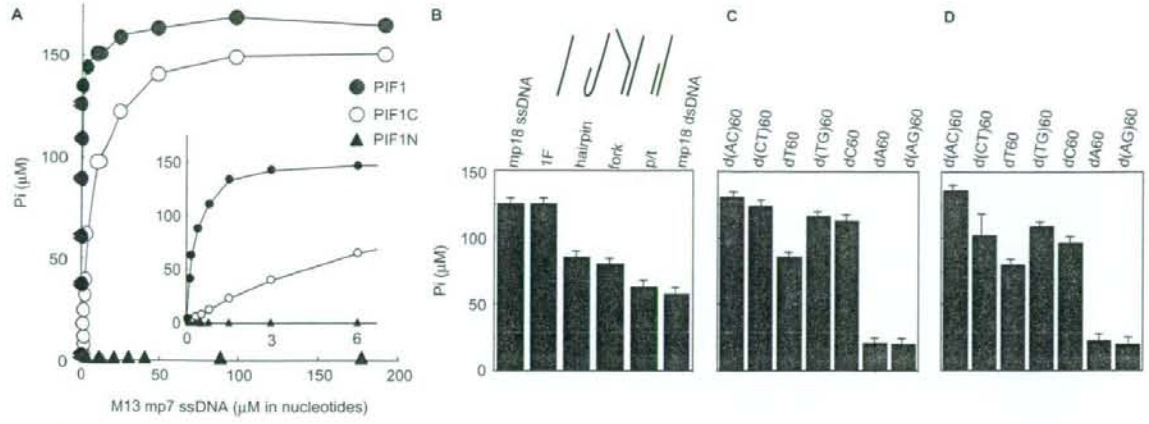

Figure 2. Effects of various DNA molecules on stimulation of ATPase activity of PIF1. **(A)** Titration of M13 mp7 ssDNA for its stimulation of ATPase activity of PIF1, PIF1N and PIF1C. ATPase activities were measured under standard reaction conditions with PIF1 proteins (13.9 nM) at 30°C for 10 min. An aliquot (2 μl) of the reaction products was then analyzed by thin layer chromatography. The extent of ATP hydrolysis was measured by determining the relative radioactivity of the released inorganic phosphate. Inset is a plot of the data at lower concentrations of ss DNA. The errors in the experiments were <10%. **(B)** Effects of the various DNA molecules on stimulation of ATPase activity of PIF1. Assays were performed with the indicated DNA (3.8 μM in nucleotides) and PIF1 (13.9 nM). **(C)** Effects of oligonucleotides with different compositions on stimulation of ATPase activity by PIF1. Assays were performed with indicated DNA (7.5 μM in nucleotides) and PIF1 (14.6 nM). **(D)** Effects of oligonucleotides with different compositions on stimulation of ATPase activity by PIF1C. Assays were performed with indicated DNA (150 μM in nucleotides), and PIF1C (13.9 nM).

K_{eff}, defined as the concentration of ssDNA required to achieve half-maximal ATP hydrolysis (5,36,37) was calculated from the titration curve (Figure 2A) using a hyperbolic curve-fitting program (Table 2). The calculated K_{eff} value, 0.35 μM (in nucleotides) for M13 mp18 ssDNA, agreed with the 0.6 μM (in nucleotides) of *Sc*Pif1 reported for the same M13 ssDNA (5).

Since PIF1 preferentially unwound the forked substrate (Figure 1), we consider that substrate specificity for unwinding activity could be correlated with stimulation of ATPase activity. To seek preferential structures for stimulation for ATPase of PIF1, we tested various DNAs, including a fork-structure, a primer-template-structure, a hairpin-structure and a linear oligonucleotide (Table 1), as well as M13 mp18 ssDNA and double stranded (ds) DNA (Figure 2B). The reactions were carried out with 3.8 μM (in nucleotides) of each oligonucleotide, which was nearly saturated concentration for M13 mp7 ssDNA (Figure 2A inset). Among these, M13 mp18 ssDNA proved to strongly and dsDNA to poorly stimulate ATPase activity (Figure 2B). Moreover, we found surprisingly that a oligonucleotide, 1F, which would not be expected to form secondary structures (Table 1), stimulated ATPase activity to the highest level, equivalent to that of M13 mp18 ssDNA (Figure 2B). The result suggested that an ssDNA region itself, rather than the structure of the DNA, is crucial for stimulation of ATPase activity of PIF1. Consequently, we compared ATPase activity stimulated by seven different 60-mer oligonucleotides composed of one or two nucleotides, guaranteed not to form secondary structures. The reactions were performed in the presence of a nearly saturated concentration of the oligonucleotides (7.5 μM in nucleotides) (Supplementary Figure S3A). The results revealed general features of ssDNA for stimulation of ATPase (Figure 2C), with the order of stimulation being poly(purine–pyrimidine) ≥ polypyrimidine ≫ polypurine.

Since these experiments were performed with nearly saturated concentrations of oligonucleotides, the results do not reflect affinities of the respective ssDNAs. We therefore determined a kinetic parameter, K_{eff}, calculated from data of ssDNA-titration experiments (Supplementary Figure S3A, data not shown) using a hyperbolic curve-fitting program (Table 2). The K_{eff} value for dsDNA was more than 20 times higher than those for ssDNA, showing a preference to ssDNA. For ssDNA, the K_{eff} values, except with polypurine, were essentially the same (~0.1 μM in nucleotides), and slightly lower than with M13 ssDNA and structured DNAs, which was probably due to over estimation of the ssDNA region because of the presence of local double-stranded regions generated by the secondary structure, since the K_{eff} values were expressed in nucleotide equivalents. These results supported our conclusion that the predominant requirement for stimulation of ATPase is nonstructural ssDNA.

Evaluation of ATPase activity of PIF1C, a mutant lacking the PINT domain

We noted that the K_{eff} value for ssDNA of PIF1 was in line with one report for *Sc*Pif1 (5), but significantly lower than that for human PIF1 with a N-terminal truncated form (4). We consider that the difference could be attributed to the missing function of the PINT domain. To test this possibility, we examined ATPase activity of PIF1C (Figure 2A), and also tested PIF1N as a control. First, we confirmed no ATPase activity of PIF1N (Figure 2A),

Table 1. Synthetic oligonucleotides used in this work

Name	Sequence
1F (73-mer)	5′-CTCCTCCTCCTCCTCCTCCTCCTCCTCCTCCTCCTCCTCCTCGCTCGACGCCATTAATAAT GTTTTC-3′
1R (73-mer)	5′-GCTCGACGCCATTAATAATGTTTTCCTCCTCCTCCTCCTCCTCCTCCTCCTCCTCCTCCTCCTCCT CCTC-3′
2L (50-mer)	5′-GAAAACATTATTAATGGCGTCGAGCTAGGCACAAGGCGAACTGCTAACGG-3′
2S (25-mer)	5′-GAAAACATTATTAATGGCGTCGAGC-3′
3F (55-mer)	5′-AGGTCTCGACTAACTCTAGTCGTTGTTCCACCCGTCCACCCGACGCCACCTCCTG-3′
3S (25-mer)	5′-CCCGTCCACCCGACGCCACCTCCTG-3′
4S (25-mer)	5′-CAGGAGGTGGCGTCGGGTGGACGGG-3′
4L (51-mer)	5′-GCAGGAGGTGGCGTCGGGTGGACGGGATTGAAATTTAGGCTGGCACGGTCG-3′
5 (fork) (55-mer)	5′-TTTTTTTTTTTTTTTTTTTTTTTTTTTTCGGACGCTCGACGCCATTAATAATGTTTTC-3′
7 (fork) (56-mer)	5′-TGAAAACATTATTAATGGCGTCGAGCGTCCGTTTTTTTTTTTTTTTTTTTTTTTTTT-3′
18 (hairpin) (73-mer)	5′-GCCTGCACGTGGCGATCGTTCGATCGCCACGTGCAGGCGCTGCTGCTGGCTCGACGCCATTAAT AATGTTTTC-3′
90 (p/t) (90-mer)	5′-TGGGCTCACGTGGTCGACGCTGGAGGTGATCACCAGATGATTGCTAGGCATGCTTTCCGCAA GAGAACGGGCGTCTGCGTACCCGTGCAG-3′
30 (p/t) (30-mer)	5′-CTGCACGGGTACGCAGACGCCCGTTCTCTT-3′
d(AC)60 (60-mer)	5′-ACACACACACACACACACACACACACACACACACACACACACACACACACACACACAC-3′
d(AG)60 (60-mer)	5′-AGAGAGAGAGAGAGAGAGAGAGAGAGAGAGAGAGAGAGAGAGAGAGAGAGAGAGAG-3′
d(TG)60 (60-mer)	5′-TGTGTGTGTGTGTGTGTGTGTGTGTGTGTGTGTGTGTGTGTGTGTGTGTGTGTGTG-3′
d(CT)60 (60-mer)	5′-CTCTCTCTCTCTCTCTCTCTCTCTCTCTCTCTCTCTCTCTCTCTCTCTCTCTCTCT-3′
d(CT)55 (55-mer)	5′-TCTCTCTCTCTCTCTCTCTCTCTCTCTCTCTCTCTCTCTCTCTCTCTCTCTCTCT-3′
d(CT)45 (45-mer)	5′-TCTCTCTCTCTCTCTCTCTCTCTCTCTCTCTCTCTCTCTCT-3′
d(CT)35 (35-mer)	5′-TCTCTCTCTCTCTCTCTCTCTCTCTCTCTCTCT-3′
d(CT)30 (30-mer)	5′-CTCTCTCTCTCTCTCTCTCTCTCTCTCTCT-3′
d(CT)20 (20-mer)	5′-CTCTCTCTCTCTCTCTCT-3′
d(CT)15 (15-mer)	5′-TCTCTCTCTCTCTCT-3′
dC60 (60-mer)	5′-CCCCCCCCCCCCCCCCCCCCCCCCCCCCCCCCCCCCCCCCCCCCCCCCCCCCCCCCCCCCCC-3′
dA60 (60-mer)	5′-AAAAAAAAAAAAAAAAAAAAAAAAAAAAAAAAAAAAAAAAAAAAAAAAAAAAAAAAAAAAAA-3′
dT60 (60-mer)	5′-TTTTTTTTTTTTTTTTTTTTTTTTTTTTTTTTTTTTTTTTTTTTTTTTTTTTTTTT-3′

Table 2. Kinetic parameters for the ATPase activity of PIF1 with various ssDNAs

DNA	PIF1 K_{eff}[a] (μM)	PIF1C K_{eff} (μM)
M13 mp7 ssDNA	0.35	8.7
M13 mp18 ssDNA	0.45	–[b]
M13 mp18 dsDNA	9.7	–
1F[c]	0.17	–
hairpin (18)[c]	0.71	–
fork (5:7)[c]	0.39	–
p/t (90:30)[c]	0.80	–
d(AC)60[c]	0.13	3.7
d(CT)60[c]	0.11	2.3
d(TG)30[c]	0.12	3.4
dT60[c]	0.11	6.4
dC60[c]	0.07	2.3
dA60[c]	1.2	nd[d]
d(AG)60[c]	1.8	nd

Kinetic assays to determine K_{eff} values were performed for 10 min in 20 μl reaction mixtures using 14 nM of PIF1 and PIF1C. Concentrations of ssDNA ranged from 0.15 to 300 μM in nucleotides. K_{eff} values were evaluated from the plot of the initial velocity versus the nucleotide concentration using a hyperbolic curve-fitting program with the correlation coefficients (R^2) more than 0.97, which were shown in supplementary Figure S3.

[a]K_{eff} is expressed in nucleotides equivalents.

[b]Not determined.

[c]Nucleotide sequences were shown in Table 1.

[d]Not detected.

as expected from the lack of any ATPase motifs. When M13 mp7 ssDNA was titrated in the reaction with PIF1C, we detected similar levels of maximum ATPase activity at higher concentrations of ssDNA (Figure 2A), suggesting that the helicase domain is sufficient to express ATPase activity. However, the required concentrations of ssDNA to achieve maximal activity were significantly increased (Figure 2A inset). The calculated K_{eff} value, 8.7 μM (in nucleotides) for M13 mp7 ssDNAs with PIF1C was more than 20 times higher than that for PIF1 (Table 2). This property was also demonstrated by determining K_{eff} values for different oligonucleotides (Table 2), calculated from data from ssDNA titration experiments (Supplementary Figure S3B). These results suggested that a defect in PIF1C could be in the binding to ssDNA, and the PINT domain could help interaction between the helicase domain and ssDNA.

To determine preferential nucleotide compositions for PIF1C stimulation of ATPase activity, it was measured using the same set of the oligonucleotides in the reactions with nearly saturated concentrations of the oligonucleotides (150 μM in nucleotides) (Supplementary Figure S3B). The results demonstrated that the preference of PIF1C was essentially identical to that of PIF1 (Figure 2C and D), suggesting that it is intrinsic to the helicase domain, the PINT domain not affecting this property.

For further comparison between PIF1 and PIF1C, we determined their K_m values for ATP in the reactions with saturating concentrations of M13 mp18 ssDNA, 3.8 and 150 μM (in nucleotides), respectively. The K_m values for ATP of both proteins were both 0.17 mM and essentially identical to the previously reported value of 0.2 mM for N-terminal-truncated human PIF1 (4). This result

suggested again that the helicase domain is sufficient to express ssDNA-dependent ATPase activity.

Characterization of ssDNA binding activities of PIF1 and PIF1C

It seemed that the apparent affinity to ssDNA for the helicase domain (PIF1C) was much lower than that for PIF1 in ATPase reactions. We considered that the defect might be attributed to binding ability to ssDNA. To measure DNA binding of PIF1 and PIF1C directly, we performed electrophoretic mobility shift assays (EMSA) using a oligonucleotide, d(AC)60 (Table 1) as a model substrate. It has been reported that this assay detects DNA–protein complexes in yeast and human PIF1 in an ATP-independent manner (7,9). Binding reactions were carried out under the optimal ATPase assay conditions, then products were loaded on gels as described in the Materials and methods section. The titration experiment displayed PIF1–DNA complexes, which were increased depending on the concentration of PIF1 (Figure 3A). The apparent K_d, which is approximately equal to the protein concentration at which half the free DNA has become bound (35), was determined to be about 3 nM. This was in good agreement with the K_{eff} value of d(AC)60 for ATPase activity, because the 0.13 μM (in nucleotides) (Table 2) corrected for the concentration of the 60-mer oligonucleotide became 2 nM.

When PIF1C was tested, we could detect PIF1C–DNA complexes, but the affinity seemed much lower than that with PIF1, demonstrating a defect in ssDNA binding activity. When the point at which half the free DNA has become bound was extrapolated from the binding curve, the apparent K_d value was estimated at about 10 nM. However, the K_d value was not directly correlated with the K_{eff} value, since it was still 6 times lower than the

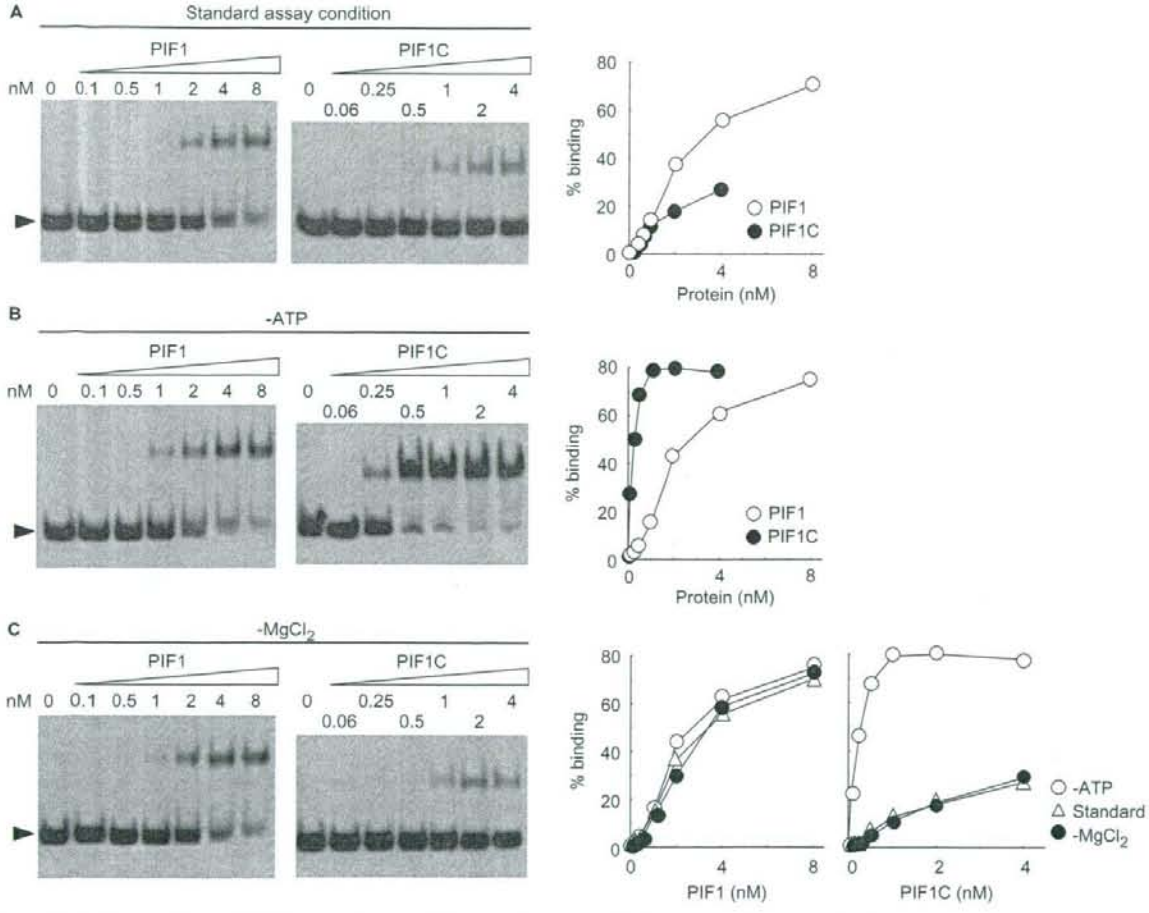

Figure 3. EMSA of PIF1 and PIF1C for binding to ssDNA. (**A**) EMSA of ssDNA binding to PIF1 and PIF1C under standard reaction conditions. The 5′-^{32}P labeled oligonucleotide, d(AC)60, was incubated with the indicated concentrations of PIF1. Arrowheads indicate the positions of free DNA. The quantified data are shown graphically. (**B**) EMSA in the absence of ATP. Experiments were performed as described in (A). The quantified data are shown graphically. (**C**) EMSA in the absence of $MgCl_2$. Experiments were performed as described in (A). The quantified data are shown graphically together with data from (A) and (B). The errors in the experiments were <10%.

apparent K_{eff} value of 60 nM (in oligonucleotides), with the K_{eff} value of 3.7 μM (in nucleotides) (Table 2), corrected for the concentration of the 60-mer oligonucleotide.

Since it was very likely that ATP could influence the binding reaction, we performed the same experiments without ATP. With the full length PIF1, the titration curve was not affected (Figure 3B). In contrast that for PIF1C in the absence of ATP was significantly changed. The apparent affinity was increased to about 0.3 nM (Figure 3B). To determine whether the effect of ATP is caused by binding or hydrolysis, titration experiments were carried out omitting $MgCl_2$ to prevent hydrolysis of ATP (Figure 3C). Under this condition, the ATPase activity was under the background level (data not shown), suggesting that, even though trace amounts of Mg ions were present as contaminants of chemicals, the contribution was negligible. The result clearly demonstrated the binding curves to be identical to that under standard assay conditions containing ATP and $MgCl_2$ (Figure 3C), suggesting that ATP binding itself affected the interaction between ssDNA and the helicase domain.

ssDNA binding activity of the PIF1N

Our results suggested that the PINT domain plays a role in modulating the ssDNA binding activity of the helicase domain. Therefore, we carried out the same binding assays with PIF1N (Figure 4A). The assays detected PIF1N–DNA complexes, and the titration curves were not affected by ATP and $MgCl_2$ (Figure 4A), with an apparent K_d value of about 10 nM. These results suggested that PIF1N itself possesses ATP-independent ssDNA binding activity.

In contrast to the binding reactions with PIF1 and PIF1C shown in Figure 3, further shifts of the mobility

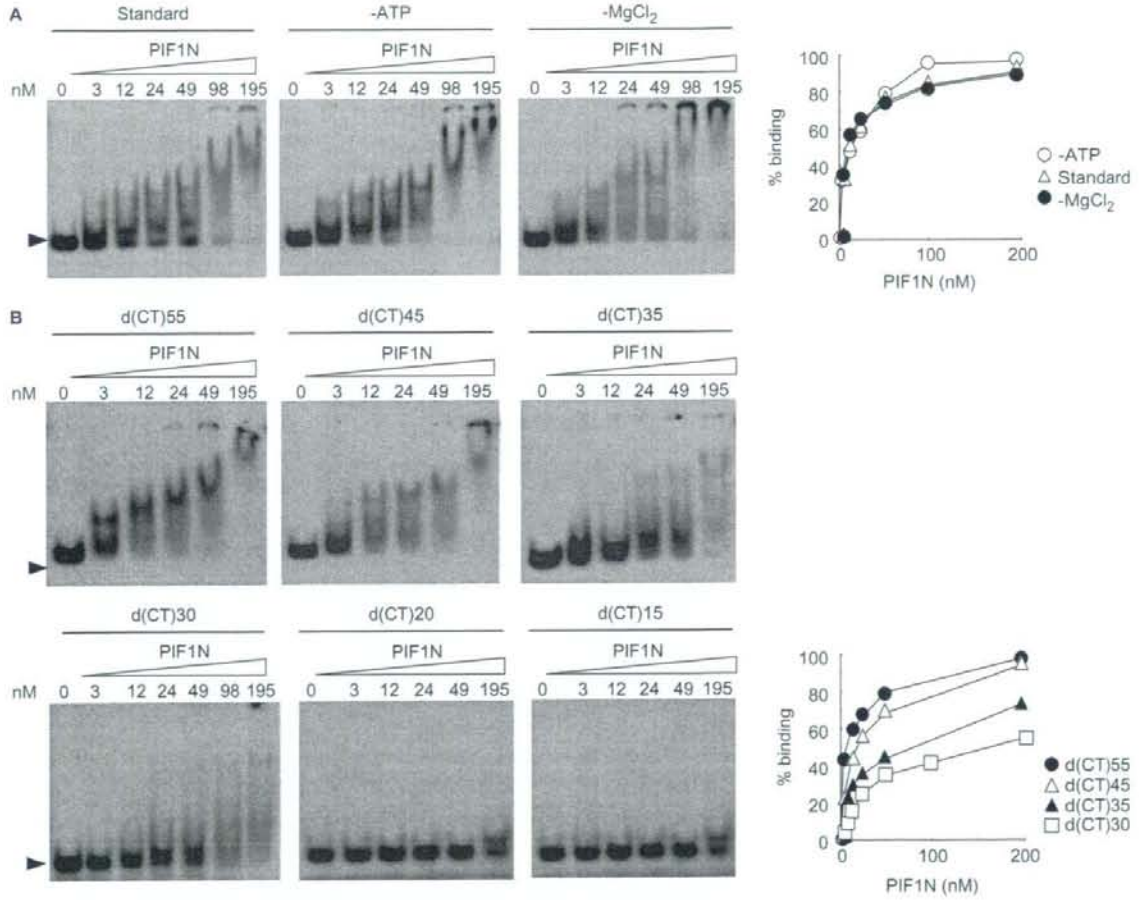

Figure 4. EMSA of PIF1N for binding to ssDNA. (**A**) Titration of PIF1N under different conditions. The 5′-^{32}P labeled oligonucleotide, d(AC)60, was incubated with the shown concentrations of PIF1N, omitting ATP or $MgCl_2$ as indicated. Arrowheads indicate the positions of free DNA. The quantified data are shown graphically. (**B**) Binding ability of PIF1N to different sizes of oligonucleotides. Experiments were performed using indicated oligonucleotides as substrates under standard reaction conditions in the absence of ATP. The quantified data are shown graphically. The errors in the experiments were <10%.

of the complexes with PIF1N in higher concentrations were observed (Figure 4A). This could be due to more than one protein molecule binding to the 60-mer oligonucleotide. To determine the minimal ssDNA size for binding of PIF1N, six different oligonucleotides in lengths ranging from 55 to 15 bases were subjected to binding assays. When the 55-mer was used as the substrate, the result was essentially identical to that for a 60-mer. However, further reduction of the length to 45-mer and 35-mer decreased the extent of multiple binding. With the 30-mer oligonucleotide, but not the 20-mer and 15-mer, a distinct band of the complex was observed. These results demonstrated that the minimal ssDNA size could be between 30 and 20 bases.

DNA strand annealing activity of PIF1, residing in the PINT domain

During helicase assays, we unexpectedly found that PIF1 possessed robust annealing activity. For detailed analysis, a forked substrate (1F:2L) (Figure 5A) was denatured by heating at 100°C for 5 min, and then incubated with PIF1 under the conditions for the standard ATPase assay omitting ATP to avoid unwinding reactions. Titration of PIF1 showed about 50% of ssDNA could be annealed within 10 min when 46 nM PIF1 was present (Figure 5B). To determine the region of PIF1 responsible for the annealing activity, PIF1C and PIF1N were tested for their ability to promote the reaction. The results demonstrated that PIF1N, but not PIF1C, efficiently annealed ssDNA, with activity only 3-fold lower than that of PIF1 when 1F and 2L substrates were tested (Figure 5B). This result indicated that the annealing activity of PIF1 resides in the PINT domain.

Since ATP is essential for helicase activity, we tested effects of ATP on the annealing reaction. To avoid the effect of unwinding, titration of ATP was carried out in the absence of $MgCl_2$. The result demonstrated both PIF1 and PIF1N to be inhibited by ATP (Figure 5C). Time course experiments demonstrated that, in the absence of ATP, PIF1 annealed up to 70% of ssDNA, whereas, in the presence of the optimal concentration of ATP (2 mM) for helicase activity, the annealed fraction reached only 20% (Figure 5D). The properties of PIF1 were same as those of PIF1N, 2 mM ATP also inhibiting annealing activity from 50% to 17% (Figure 5E). Importantly, the ATP-titration curve and time course with PIF1 were essentially identical to those for PIF1N (Figure 5C–E), suggesting that the properties are intrinsic to the PINT domain.

Further confirming this conclusion, we used completely complementary strands as a substrate. The annealing product has no ssDNA region, preventing product unwinding under the standard reaction conditions containing ATP and $MgCl_2$. Titration curves of ATP for PIF1 and PIF1N demonstrated again inhibitory effects, although significant fractions of the substrates were spontaneously annealed under the assay conditions (Figure 5F).

Effects of RPA on unwinding and annealing reactions of PIF1

Elucidation of whether PIF1 has the potential to promote unwinding and annealing reactions on RPA-coated substrates is valuable for understanding cellular functions of PIF1. To do this, first, we determined the optimal concentration of RPA for the substrate DNA binding by EMSA. The substrate, 3F:4L was used for the binding reactions at the final concentration of 0.35 nM. The results of titration of RPA are shown in Figure 6A. When the concentration of RPA was increased to 0.9 nM, one molecule of RPA bound to at least one strand of the forked substrate. At >1.8 nM, each strand of the substrate was probably occupied by one RPA molecule (Figure 6A). The levels of apparent affinity of RPA for ssDNA were in good agreement with previous reports (38).

Then we examined unwinding activity of PIF1. RPA was mixed with the forked substrate, 3F:4L, under the standard reaction conditions on ice, then PIF1 was introduced and incubation was performed at 30°C for 10 min. We found that RPA did not affect unwinding reactions at low concentrations <0.4 nM (Figure 6B, left panel), in which majority of the substrate was RPA-free (Figure 6A). When the concentration of RPA reached 0.9 nM, at which almost all the oligonucleotides were occupied with RPA (Figure 6A), severe inhibition was observed (Figure 6B, left panel). At much higher concentrations of RPA, we observed unwinding products (Figure 6B, left panel). However, a control experiment without PIF1 revealed that the products detected at higher concentrations >1.8 nM of RPA were PIF1 independent (Figure 6B, right panel). The quantified results shown in Figure 6C demonstrate no difference in the two reactions at higher concentrations of RPA (>0.9 nM). These results suggest that RPA does not enhance, but rather inhibits, the helicase activity of PIF1.

To examine annealing activity in the presence of RPA, we also determined the optimal concentration of RPA for ssDNA binding. In the reactions, we used the same substrate as for the unwinding assay (3F:4L) at the final concentration of 0.35 nM, but after denaturation by heating. The assay detected only complexes with the labeled oligonucleotide 3F (55-mer), although another fragment, 4L (51-mer), was present. The results of titration of RPA are shown in Figure 6D. When the concentration of RPA was increased to 0.9 nM, almost all the oligonucleotides 3F and probably 4L were occupied by at least one molecule of RPA. At >1.8 nM, the oligonucleotides were occupied by two molecules of RPA (Figure 6D).

Next, we carried out annealing assays under the same conditions. RPA was mixed with heat denatured substrate (3F and 4L) on ice, then PIF1 was introduced with incubation at 30°C for 10 min. The result clearly demonstrated an inhibitory effect of RPA (Figure 6E). The quantified results for inhibition of annealing reactions well correlated inversely with the amount of RPA binding (Figure 6F).

DISCUSSION

In this article, we document for the first time the biochemical properties of full-length human PIF1 together with those of truncated forms consisting of individual domains. We could establish intrinsic properties of the helicase domain and functional roles of the PINT domain.

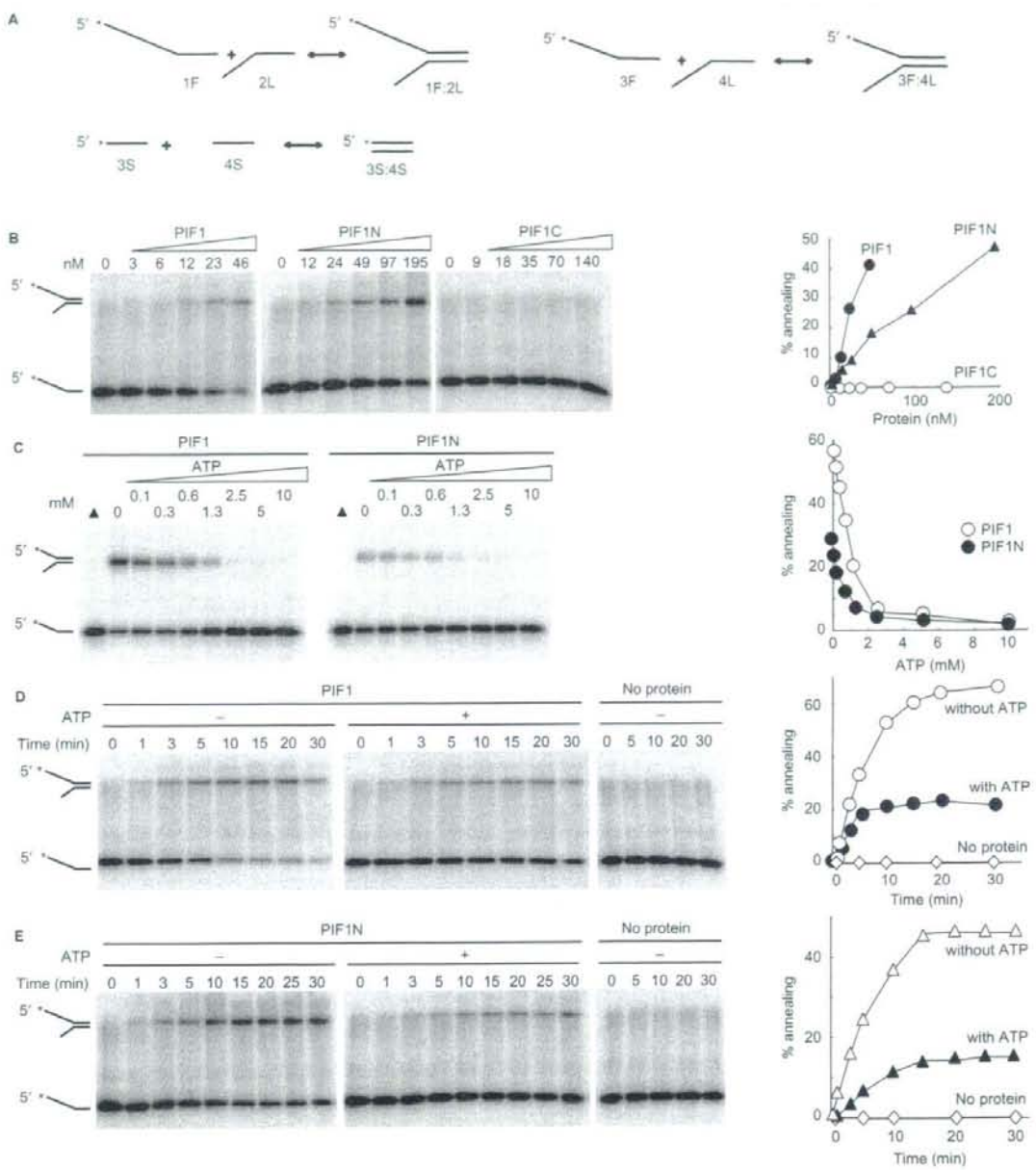

Figure 5. DNA strand annealing activity. (**A**) Schematic structures of the DNA substrates. The asterisks indicate ^{32}P-labeled 5′-phosphate. (**B**) Annealing activities of PIF1, PIF1C and PIF1N. The fork-structural partial duplex DNA substrate, 1F:2L (0.35 nM), was boiled for 5 min, then incubated with increasing levels of PIF1, PIF1C and PIF1N as indicated under standard reaction conditions omitting ATP at 30°C for 10 min. The quantified data are shown graphically. (**C**) Titration of ATP on annealing reactions mediated by PIF1 and PIF1N. The fork-structural partial duplex DNA substrate, 3F:4L (0.35 nM), was boiled for 5 min, then incubated with PIF1 (33 nM) or PIF1N (195 nM) and increasing levels of ATP under standard reaction conditions omitting $MgCl_2$ at 30°C for 10 min. The quantified data are shown graphically. (**D**) Time course of annealing reactions mediated by PIF1 under standard reaction conditions omitting $MgCl_2$. Heat denatured substrate DNA, 1F:2L (0.35 nM), was incubated with PIF1 (46 nM). The quantified data are shown graphically. (**E**) Time course of annealing reactions mediated by PIF1N under standard reaction conditions omitting $MgCl_2$. Heat denatured substrate DNA, 1F:2L (0.35 nM), was incubated with PIF1N (195 nM). The quantified data are shown graphically. (**F**) Titration of ATP on annealing reactions mediated by PIF1 and PIF1N under standard reaction conditions. A complete double stranded oligonucleotide, 3S:4S (0.35 nM) was boiled for 5 min, then incubated with PIF1 (30 nM) or PIF1N (195 nM) and increasing levels of ATP under standard reaction conditions at 30°C for 10 min. The quantified data are shown graphically. The errors in the experiments were <10%.

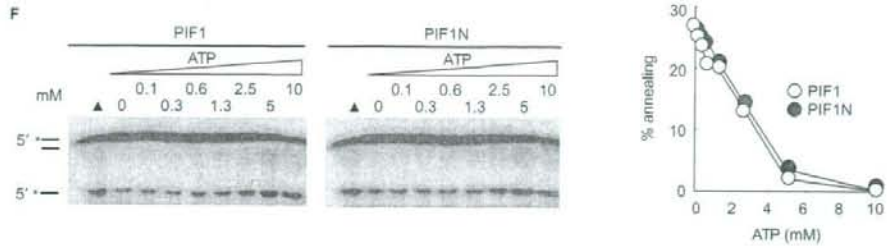

Figure 5. Continued.

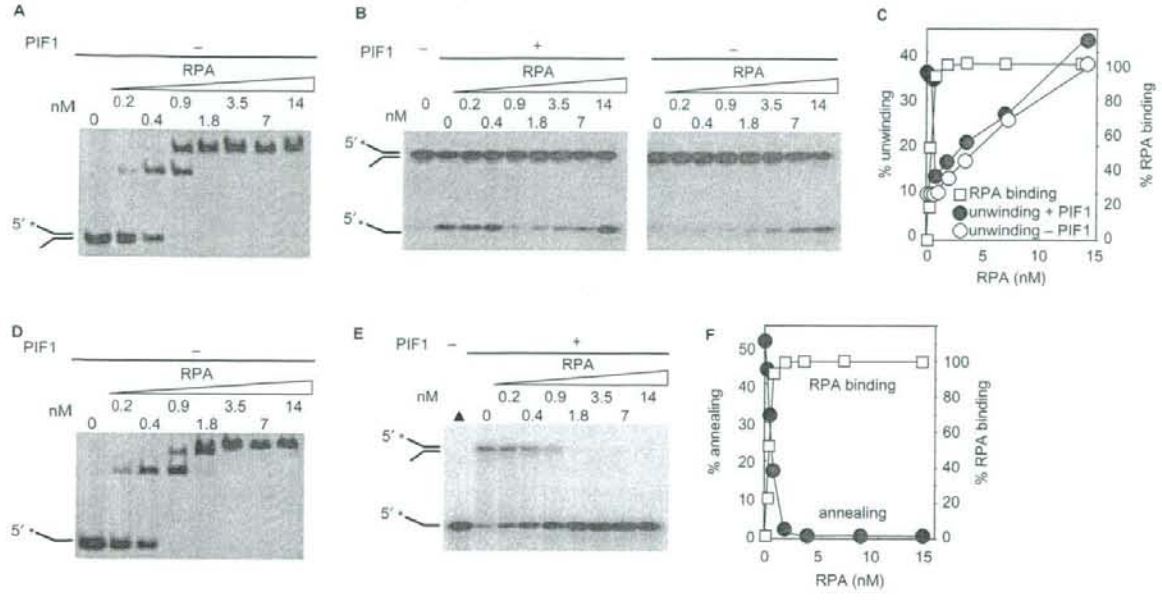

Figure 6. Effects of RPA on the unwinding and annealing reactions. **(A)** EMSA of RPA binding. The fork-structural partial duplex DNA substrate, 3F:4L (0.35 nM) was incubated with RPA at indicated concentrations on ice for 10 min under the standard reaction conditions. **(B)** Unwinding assay in the presence of RPA. The fork-structural partial duplex DNA substrate, 3F:4L (0.35 nM), was incubated with RPA at indicated concentrations on ice for 10 min under standard reaction conditions. Then, PIF1 (16 nM) (left panel) and buffer (right panel) were introduced and incubated at 30°C for 10 min. Reaction products were separated on a 15–25% polyacrylamide gel. **(C)** The quantified data of unwinding reactions in (B) are shown graphically with the RPA binding curve in (A). **(D)** EMSA of RPA binding. The fork-structural partial duplex DNA substrate, 3F:4L (0.35 nM), was boiled for 5 min, then incubated with RPA at indicated concentrations on ice for 10 min under the standard reaction conditions omitting ATP. **(E)** Annealing assay in the presence of RPA. The fork-structural partial duplex DNA substrate, 3F:4L (0.35 nM) (Figure 5A), was boiled for 5 min, then incubated with RPA at indicated concentrations on ice for 10 min under standard reaction conditions omitting ATP. Then PIF1 (30 nM) was introduced and incubated at 30°C for 10 min. Reaction products were separated on a 15–25% polyacrylamide gel. **(F)** The quantified data of annealing reactions in (E) are shown graphically with the RPA binding curve in (D). The errors in the experiments were <10%.

Biochemical analysis of yeast PIF1 homologs has demonstrated that they preferentially unwind forked substrates (1,5,7). We showed that the property is conserved in human PIF1. However, we found that forked substrates were not optimal with respect to stimulation of ATPase activity. Rather nonstructural ssDNA greatly stimulated ATPase activity. The finding that the K_{eff} value for nonstructural ssDNA was lower than for other DNA molecules, including forked structures, suggested preferential binding of PIF1 to ssDNA. From these results, we suggest that PIF1 needs an ssDNA region for loading and a forked structure for entrance to the double strand region by translocation.

We present several lines of evidence that the enzymatic characters of PIF1C reflect the intrinsic properties of the helicase domain. First, PIF1C expressed ATPase activity to the level equivalent to full-length PIF1 (about 1000 min^{-1}) and also equivalent to that for yeast homologs (5,7). Second, full-length PIF1 and PIF1C both showed a similar preference for poly(purine–pyrimidine) and polypyrimidine, but not polypurine, for stimulation of ATPase. This property is also conserved in yeast homologs (5,7). Third, the K_m values for ATP of full-length PIF1 and PIF1C were essentially identical. This is also in agreement with a previous report for N-terminal truncated PIF1, purified as a C-terminus GST-fusion protein (4).

These results suggest that the determined properties of PIF1C are intrinsic to the helicase domain, and could also exclude the possibility that the his-tag at the N-terminal of PIF1C interferes with activities of the helicase domain.

Interestingly, we noted a significant difference between PIF1 and PIF1C with regard to the required concentration of ssDNA for stimulation of ATPase activity. PIF1C needed a 20 times higher concentration and also exhibited much lower unwinding activity. The results suggest that the defects could be attributed to missing functions of the PINT domain. The difference in the K_{eff} values could be due to lower binding affinity of the helicase domain for ssDNA. Consequently, we demonstrated ssDNA binding of PIF1 directly by EMSA. The apparent K_d value, 3 nM was in good agreement with the K_{eff} value of 2 nM when expressed with reference to the oligonucleotide concentration, suggesting that this assay well reflected the functional interaction between ssDNA and PIF1. In this assay, as expected, we demonstrated lower affinity of PIF1C to ssDNA. We suggested that the defect in PIF1C could be due, at least in part, to lower binding affinity for ssDNA, and the PINT domain plays a role for increasing this affinity of the helicase domain. Notably, the K_d value (10 nM) of PIF1C determined by EMSA was still 6 times lower than the K_{eff} value (60 nM in oligonucleotides) for the ATPase assay. We consider the following possible explanations for the discrepancy. We found that PIF1C exhibited a much higher affinity for ssDNA without binding of ATP. With the EMSA, an ATP-free fraction of PIF1C could exist, even in the presence of ATP. Therefore, the results could be an overestimation, due to high affinity binding of the ATP-free fraction of PIF1C. Alternatively, the PINT domain could possess another function for enhancing activity of the helicase domain by modulating the mode of interaction with ssDNA. The higher affinity of PIF1C for ssDNA without binding of ATP could be intrinsic to the helicase domain. The results suggested that ATP modulated the binding mode with ssDNA. The higher affinity to ssDNA before binding of ATP is reduced by binding of ATP. The alteration must be alternatively repeated during turnover of reactions of ATPase. With the full-length PIF1, such alteration due to ATP binding was not detected, suggesting that the PINT domain somehow could suppress the alteration during turnover of ATPase reactions. In this study, we demonstrated that the PINT domain also possesses ssDNA binding activity. We suggest that its enhancement of the activities of the helicase domain is due, at least in part, to this ssDNA binding activity.

We unexpectedly found the PINT domain to further possess ssDNA annealing activity. Among the proteins handled in this study having ssDNA binding activity, including PIF1C, PIF1N and RPA, we could detect annealing activity only with PIF1N. We consider that the annealing activity could be mediated by ssDNA binding, although not attributable to the general effect of high affinity ssDNA binding. Annealing activity has been reported to be associated with the RecQ family helicase in general (39–45). While the RecQ family is distinct from PIF1 family, annealing activity shares similar properties in common. It is located outside of the conserved helicase domains (39,40), is inhibited by RPA, and is ATP-independent or rather inhibited by ATP (39–42,44). We demonstrated that inhibition by ATP is not a consequence of the unwinding reaction, suggesting that it is an intrinsic property of the PINT domain.

At the present time, the biological significance of our findings cannot be readily assessed. Importantly, we showed that RPA inhibited unwinding and annealing reactions, suggesting that these functions of PIF1 might be restricted under particular situations in DNA metabolism. There is a marked difference from RecQ helicases, whose unwinding activity is proficient on RPA-coated ssDNA and stimulated by RPA, although annealing activity is suppressed (39–41,46–48). Notably, unwinding activity of *Sc*Pif1 was stimulated by RPA (1), but that of the fission yeast homolog, Pfh1, was inhibited (7) like human PIF1, suggesting that the outcomes in cells would differ. This could be related to the fact that budding yeast has another member of the PIF1 superfamily, Rrm3, but human and fission yeast have only one. Further analysis of the precise cellular roles of PIF1 should shed light on functions in maintenance of genetic stability.

SUPPLEMENTARY DATA

Supplementary Data are available at NAR Online.

ACKNOWLEDGEMENTS

We thank Dr Marc S. Wold (University of Iowa College of Medicine, Iowa City, Iowa, USA), Dr Hisaji Maki (Nara Institute of Science and Technology, Nara, Japan) and Dr Tadashi Shimamoto (Hiroshima University, Hiroshima, Japan) for, respectively, providing an RPA-expression plasmid, the M13 mp7 plasmid and the *E. coli* strain to produce ss M13 DNA. Several cloning vectors were obtained from National BioResource Project (NIG, Japan). We are grateful to Kumiko Mizuno, Tomoka Nakashima, Masako Okii, Fumie Okubo, Kazumi Shimamoto, Hatsue Wakayama and Mai Yoshida for their laboratory assistance.

FUNDING

Grants-in-Aid from the Ministry of Education, Culture, Sports, Science and Technology of Japan (to Y.M. and K.K.); 21st Century Center of Excellence Program from the Ministry of Education, Culture, Sports, Science and Technology of Japan (to K.K.); Health and Labour Science Research Grants (to K.K.); Grants-in-Aid for Cancer Research from the Ministry of Health, Labour and Welfare (to K.K.). Funding to pay the Open Access publication charges for this articles was provided by Grant-in-Aid from the Ministry of Education, Culture, Sports, Science and Technology of Japan (to Y.M.).

Conflict of interest statement. None declared.